Acta Pharmaceutica Sinica B 2021;11(2):373−393

Chinese Pharmaceutical Association
Institute of Materia Medica, Chinese Academy of Medical Sciences

Acta Pharmaceutica Sinica B

www.elsevier.com/locate/apsb
www.sciencedirect.com

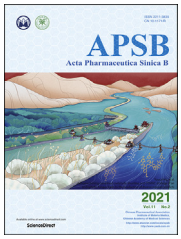

REVIEW

Recent developments on PET radiotracers for TSPO and their applications in neuroimaging

Lingling Zhang[a,b,†], Kuan Hu[c,†], Tuo Shao[d], Lu Hou[a], Shaojuan Zhang[a], Weijian Ye[a], Lee Josephson[d], Jeffrey H. Meyer[e], Ming-Rong Zhang[c], Neil Vasdev[d,e], Jinghao Wang[f], Hao Xu[a,*], Lu Wang[a,d,*], Steven H. Liang[d,*]

[a]*Center of Cyclotron and PET Radiopharmaceuticals, Department of Nuclear Medicine and PET/CT-MRI Center, The First Affiliated Hospital of Jinan University, Guangzhou 510630, China*
[b]*Department of Neurology, the First Affiliated Hospital of Jinan University, Guangzhou 510630, China*
[c]*Department of Radiopharmaceuticals Development, National Institute of Radiological Sciences, National Institutes for Quantum and Radiological Science and Technology, Chiba 263-8555, Japan*
[d]*Division of Nuclear Medicine and Molecular Imaging, Massachusetts General Hospital & Department of Radiology, Harvard Medical School, Boston, MA 02114, USA*
[e]*Azrieli Centre for Neuro-Radiochemistry, Brain Health Imaging Centre, Centre for Addiction and Mental Health & Department of Psychiatry, University of Toronto, Toronto ON M5T 1R8, Canada*
[f]*Department of Pharmacy, the First Affiliated Hospital of Jinan University, Guangzhou 510630, China*

Received 17 April 2020; received in revised form 15 July 2020; accepted 29 July 2020

Abbreviations: AD, Alzheimer's disease; ALS, amyotrophic lateral sclerosis; Am, molar activities; AMPA, α-amino-3-hydroxy-5-methyl-4-isoxazole propionic acid; ANT, adenine nucleotide transporter; BBB, blood–brain barrier; *Bc*TSPO, *Bacillus cereus* TSPO; BMSC, bone marrow stromal cells; BP, binding potential; BP_{ND}, non-displaceable binding potential; CBD, corticobasal degeneration; CNS, central nervous system; CRAC, cholesterol recognition amino acid consensus sequence; d.c. RCYs, decay-corrected radiochemical yields; DLB, Lewy body dementias; dMCAO, distal middle cerebral artery occlusion; EP, epilepsy; f_p, plasma free fraction; FTD, frontotemporal dementia; HAB, high-affinity binding; HD, Huntington's disease; HSE, herpes simplex encephalitis; IMM, inner mitochondrial membrane; KA, kainic acid; LAB, low-affinity binding; LPS, lipopolysaccharide; MAB, mixed-affinity binding; MAO-B, monoamine oxidase B; MCI, mild cognitive impairment; MDD, major depressive disorder; MMSE, mini-mental state examination; MRI, magnetic resonance imaging; MS, multiple sclerosis; MSA, multiple system atrophy; NAA/Cr, *N*-acetylaspartate/creatine; n.d.c. RCYs, non-decay-corrected radiochemical yields; OCD, obsessive compulsive disorder; OMM, outer mitochondrial membrane; PAP_7, RIa-associated protein; PBR, peripheral benzodiazepine receptor; PCA, posterior cortical atrophy; PD, Parkinson's disease; PDD, PD dementia; PET, positron emission tomography; p.i., post-injection; PKA, protein kinase A; PpIX, protoporphyrin IX; PRAX-1, PBR-associated protein 1; PSP, progressive supranuclear palsy; P2X7R, purinergic receptor $P2X_7$; QA, quinolinic acid; RCYs, radiochemical yields; ROS, reactive oxygen species; RRMS, relapsing remitting multiple sclerosis; SA, specific activity; SAH, subarachnoid hemorrhage; SAR, structure−activity relationship; SCIDY, spirocyclic iodonium ylide; SNL, selective neuronal loss; SNR, signal to noise ratio; SUV, standard uptake volume; SUVR, standard uptake volume ratio; TBAH, tetrabutyl ammonium hydroxide; TBI, traumatic brain injury; TLE, temporal lobe epilepsy; TSPO, translocator protein; VDAC, voltage-dependent anion channel; V_T, distribution volume.

*Corresponding authors.
E-mail addresses: txh@jnu.edu.cn (Hao Xu), l_wang1009@jnu.edu.cn (Lu Wang), liang.steven@mgh.harvard.edu (Steven H. Liang).
†These authors make equal contributions to this work.

Peer review under responsibility of Chinese Pharmaceutical Association and Institute of Materia Medica, Chinese Academy of Medical Sciences.

https://doi.org/10.1016/j.apsb.2020.08.006

KEY WORDS

TSPO;
Microglial activation;
Neuroinflammation;
Positron emission tomography (PET);
CNS disorders

Abstract The 18 kDa translocator protein (TSPO), previously known as the peripheral benzodiazepine receptor, is predominately localized to the outer mitochondrial membrane in steroidogenic cells. Brain TSPO expression is relatively low under physiological conditions, but is upregulated in response to glial cell activation. As the primary index of neuroinflammation, TSPO is implicated in the pathogenesis and progression of numerous neuropsychiatric disorders and neurodegenerative diseases, including Alzheimer's disease (AD), amyotrophic lateral sclerosis (ALS), Parkinson's disease (PD), multiple sclerosis (MS), major depressive disorder (MDD) and obsessive compulsive disorder (OCD). In this context, numerous TSPO-targeted positron emission tomography (PET) tracers have been developed. Among them, several radioligands have advanced to clinical research studies. In this review, we will overview the recent development of TSPO PET tracers, focusing on the radioligand design, radioisotope labeling, pharmacokinetics, and PET imaging evaluation. Additionally, we will consider current limitations, as well as translational potential for future application of TSPO radiopharmaceuticals. This review aims to not only present the challenges in current TSPO PET imaging, but to also provide a new perspective on TSPO targeted PET tracer discovery efforts. Addressing these challenges will facilitate the translation of TSPO in clinical studies of neuroinflammation associated with central nervous system diseases.

1. Introduction

The 18 kDa translocator protein (TSPO)[1], first described as the peripheral benzodiazepine receptor (PBR), is mainly expressed in the outer mitochondrial membrane (OMM), in particular at the interface between OMM and inner mitochondrial membrane (IMM)[2]. TSPO has 169 amino acids and consists of five transmembrane α-helix domains, which are joined by two extramitochondrial and intramitochondrial loops, an extramitochondrial C-terminal, and an intramitochondrial N-terminal. The first and third loops are located on the cytoplasmic side of the membrane, while the second and fourth loops face the inside of the mitochondria[3] (Fig. 1). Li et al.[4] first described a cholesterol recognition amino acid consensus sequence (CRAC) in the C-terminus of TSPO, which was determined to be helical in conformation from amino acids L144 to S159[5]. CRAC, together with a groove in TSPO, can bind a cholesterol molecule and is thus responsible for cholesterol transport[4,5] (Fig. 1). TSPO generally functions as a monomer[6], but it has been demonstrated to form oligomeric compounds with itself (homo-oligomer) or other proteins, such as a 32 kDa voltage-dependent anion channel (VDAC) and a 30 kDa adenine nucleotide transporter (ANT)[7]. Additionally, increased levels of reactive oxygen species (ROS) can facilitate covalent binding among TSPO monomers, inducing the formation of TSPO oligomers[8]. TSPO monomers can recognize cholesterol, and TSPO homo-oligomers may also play an important role in binding and transporting cholesterol[7]. TSPO is rich in tryptophan, a feature that is highly conserved from bacteria to mammals. Guo et al.[9] recently reported the complex crystal structure of *Bacillus cereus* TSPO (*Bc*TSPO) with its inhibitor, PK11195, at a resolution down to 1.7 Å. These authors also described similar TSPO protoporphyrin IX (PpIX)-directed catalytic activities in both *Xenopus* and humans, demonstrating the physiological importance of TSPO in protection against oxidative stress. Subsequently, Li et al.[10] described the crystal structures (at 1.8, 2.4, and 2.5 Å resolution) for TSPO from *Rhodobacter sphaeroides* and a mutant *TSPO* that simulated the human *rs6971* polymorphism ($Ala^{147} \rightarrow Thr^{147}$). The *A147T* mutation in humans perturbs the environment around the CRAC site and could transform the TSPO cholesterol-binding surface. Additionally, variation in the tilt of the helices leads to decreased binding with other ligands, indicating that the *A147T* mutation causes a lower-affinity conformational change.

TSPO is responsible for the translocation of cholesterol from the outer to the inner mitochondrial membrane, thereby limiting the rate of neurosteroid biosynthesis[11]. In addition, TSPO is also involved in other physiological functions including immunomodulation[12], mitochondrial metabolism and function[13], apoptosis[14], cell respiration and oxidative processes[15], cell proliferation and differentiation[16], protein import[17], porphyrin transport and heme biosynthesis[18], and ion transport[19] (Fig. 1). Under physiological conditions, TSPO is widely distributed throughout the body with the highest concentrations observed in steroidogenic tissues. It is predominantly expressed in the kidneys, nasal epithelium, adrenal glands, lungs, and heart, while organs such as the brain and liver show relatively low expression[1]. However, TSPO has been shown to be involved in brain ischemia-reperfusion injury[20], neurodegenerative diseases[21], and other diseases[22,23]. In the central nervous system (CNS), TSPO expression is strongly upregulated in activated microglial cells by inflammatory stimuli[24]. Lavisse et al.[25] found that reactive astrocytes also overexpress TSPO. Furthermore, activated peripheral macrophages sometimes express TSPO[26], so in theory, under conditions of compromised blood–brain barrier (BBB) peripheral macrophages could infiltrate the brain. Abnormal TSPO expression in glial cells[27,28] is implicated in the progression of neuropsychiatric disorders involving neuroinflammation including Alzheimer's disease (AD), amyotrophic lateral sclerosis (ALS), Parkinson's disease (PD), and multiple sclerosis (MS)[27,28]. As a result, TSPO is considered to be a

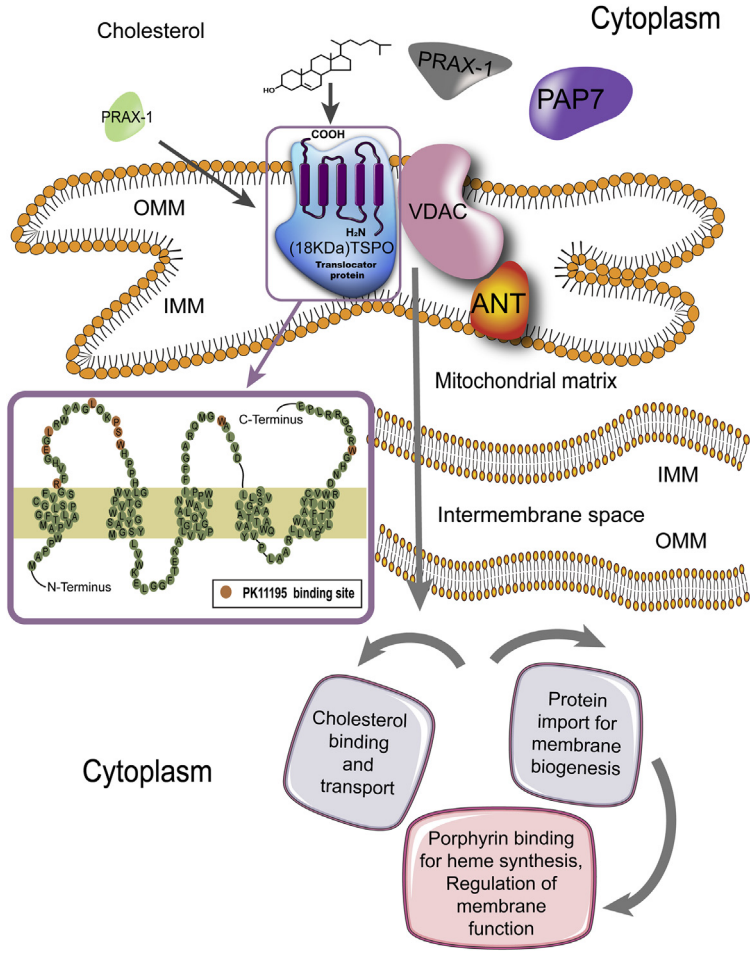

Figure 1 TSPO structure and function. TSPO is mainly expressed in the OMM with five transmembrane alpha helix domains. The topology of TSPO in the membrane is amplified, with amino acids involved in the binding site of PK11195 highlighted. The PK11195 binding site includes the residues R24, E29, L31, L37, P40, S41, W42, W107 and W161. TSPO generally functions as a monomer, but can also form compounds with itself or other proteins, such as VDAC and ANT. Furthermore, PBR-associated protein 1 (PRAX-1), and PBR and protein kinase A (PKA) regulatory subunit RIa-associated protein (PAP7) are correlated with TSPO. PRAX-1 and PAP7 could also promote compound formation or cholesterol targeting to TSPO. TSPO has four dominating functions: (1) binding and transporting cholesterol, a critical function in neurosteroid synthesis and bile salt biosynthesis; (2) protein transport for membrane biosynthesis and other important physiological functions including cell proliferation, differentiation, and apoptosis; (3) binding and importing porphyrin for heme biosynthesis; and (4) adjusting mitochondrial functions.

promising biomarker for neuroinflammation that could be used for monitoring the effectiveness of anti-inflammatory therapies[29,30].

Positron emission tomography (PET) is a noninvasive imaging technology which can provide quantitative biological information *in vivo*, and plays an important role in disease diagnosis, therapy assessment and drug development[31–33]. Unlike anatomical imaging techniques such as X-ray, ultrasound and magnetic resonance imaging (MRI), PET offers the real-time biological processes in molecular level based on a specific ligand bearing a positron-emitting radionuclide ("PET tracer"), which makes this technology with high sensitivity and excellent tissue penetration[34]. The commonly used positron radionuclides consist of ^{11}C ($t_{1/2}$ = 20.4 min),^{18}F ($t_{1/2}$ = 109.7 min), ^{68}Ga ($t_{1/2}$ = 67.6 min), ^{64}Cu ($t_{1/2}$ = 12.8 h) and ^{89}Zr ($t_{1/2}$ = 78.4 h)[35], the former two isotopes are most widely used for labeling small organic molecules[36,37], while the metal radionuclides are more feasible to label peptide[38,39], antibody[40,41] and nano materials[42]. Another advantage of PET is that the amount of radiotracer used in imaging studies is very low (10^{-6}–10^{-9} g; microdosing), which is feasible to evaluate the biological process without pharmacological effects, as well as to enable rapidly translation of promising radiotracers from bench work to phase 0 clinical trials[43].

A number of radioligands have been developed for visualizing TSPO biodistribution and expression in physiological and pathological conditions, as well as for determining the relationship between TSPO quantification and disease progression[44]. Representative TSPO PET tracers advancing into human brain imaging study as well as the clinical data are summarized in Supporting Information Table S1 (the corresponding structures of tracers are depicted in the following figures) [^{11}C]PK11195, the first prototypical PET tracer for TSPO, has historically been the most widely used to monitor neuroinflammation in various neurological disorders[45–48]. However [^{11}C]PK11195 has a relatively low signal to noise ratio (SNR) due to high nonspecific binding, and the short half-life of ^{11}C (20.4 min) limits widespread transportation and clinical trials. Therefore, there have been many efforts to develop new radioligands with improved pharmacokinetics and imaging quality, and several next-generation TSPO radioligands have been

developed for more accurate visualization of TSPO[49−53]. Although these new PET tracers show improved SNR, there is a limitation that there is variability in TSPO binding potential (BP) among individuals due to a single nucleotide polymorphism in the *TSPO* gene[54]. The human *TSPO* gene is located on chromosome 22q13.3, consists of four exons, and encodes 169 amino acids[55]. Recent studies discovered a single-nucleotide polymorphism (*rs6971*) in exon 4 of the human *TSPO* gene that results in a nonconservative alanine to threonine substitution, influencing the TSPO protein's ligand binding affinity[56]. The *rs6971* polymorphism can lead to three distinct binding statuses: high-, mixed-, and low-affinity binders. The main form, Ala/Ala, is correlated with high-affinity binding (HAB), while the Ala/Thr form has mixed-affinity binding (MAB), and the Thr/Thr form has low-affinity binding (LAB)[57]. This gene polymorphism can influence the binding affinities of almost all of the second-generation TSPO tracers, requiring inclusion of the HAB and MAB distinction as a covariate in analyses, and exclusion of LAB participants in human clinical studies. The frequency of the polymorphisms varies by ethnic background such that the LAB frequency ranges from approximately 1 in 10 Caucasians to about 10-fold less in East Asians (http://hapmap.ncbi.nlm.nih.gov/). Therefore, the development of novel radioligand candidates that are insensitive to the *rs6971* polymorphism, namely third-generation PET tracers, would enable greater inclusion of participants for TSPO imaging in human studies.

Here, we assess the most recent developments in TSPO PET tracers, as well as recent pharmacological developments, such as new-generation PET tracers. In this review, we will introduce the newest TSPO radioligands and discuss the challenges in TSPO radioligand development. Since there are no clinically approved TSPO PET tracers, we will also focus on new opportunities for radioligand development in alignment with recent drug discovery campaigns.

2. TSPO in the brain

Microglia are resident macrophages in the brain as well as resident CNS immune cells that form the first line of defense against invading pathogens and other harmful agents. Approximately 15% of the non-neuronal cells in the CNS are microglia[58]. They exquisitely monitor the brain milieu and can rapidly produce factors that affect surrounding neurons and astrocytes. Activated microglia and astroglia are often important participants in neuroinflammation[59]. Under physiological conditions, microglia usually exhibit a resting phenotype in which they are highly sensitive to changes in the brain microenvironment and can quickly switch to an activated phenotype in response to infection or injury[60,61]. After activation, microglia proliferate and migrate to the injured part, adopting typical morphological and functional properties[62]. The activated microglia exhibit morphological changes which may include shortening and thickening of their cellular processes, undergoing hypertrophy of the cell body or even changing to an ameboid state. In the resting state, microglia can secrete various growth factors and produce factors that support tissue maintenance[63,64]. When injury and/or inflammatory factors are released, microglia change from a resting state to an activated state. This activated state can include pro-inflammatory or anti-inflammatory functions or a combination of both[65].

Previous studies have observed increased TSPO expression levels under neuroinflammatory conditions[28,66,67]. TSPO is highly expressed in activated microglia, but expressed at much lower levels in "resting" or surveying microglia found mainly in the gray matter[27,28]. The dramatic upregulation of TSPO has been reported to coincide with microglial activation in response to brain injury or inflammation[68,69]. Thus, TSPO has been considered a hallmark of neuroinflammation.

The increase of TSPO levels after the injury of brain are mainly occurred in the primary or secondary regions of injury that express activated glial cells. Importantly, TSPO can be visualized and quantified using *in vitro* and *in vivo* imaging techniques. TSPO PET tracers have been used to both improve knowledge about the effect of neuroinflammation on CNS disorders and to the efficacy of new anti-inflammatory treatment strategies. Currently, TSPO PET imaging is the most widely used *in vivo* method for inferring on the status of microglial activation. Direct evidence for an innate inflammatory response in AD was described nearly 20 years ago[70], and subsequent studies have demonstrated neuroinflammation in PD[71], ALS[72,73], MS[74], major depressive disorder (MDD)[30], obsessive compulsive disorder (OCD)[75] and a growing number of other nervous system pathologies. Previous studies in rodents after lipopolysaccharide (LPS) or toxins have also reported that dramatic upregulation of TSPO levels are correlated with microglial activation in response to brain injury or neuroinflammation[76,77] although in postmortem investigations in humans both activated microglia and astroglia may overexpress TSPO[27,28].

3. Development of radioligands targeting TSPO

The development of PET tracers for brain imaging usually commence with medicinal chemistry and pharmacological screening of potential TSPO ligands aimed for high binding affinity and high selectivity[78−80]. After carefully exploration of the structure−activity relationship (SAR), the candidate PET ligand is selected and amenable for $^{11}C/^{18}F$ radiolabeling, specifically focusing on the preparation of precursors, optimization of labeling conditions, as well as translational study using automatic synthesis modules. The radiolabeling reaction of each TSPO PET tracer is depicted in Supporting Information Scheme S1. ^{11}C labeling was conventionally conducted in the presence of base such as NaOH, NaH or tetrabutyl ammonium hydroxide (TBAH), with phenol or amide as the precursor. The labeling was straightforward, and the ^{11}C-labeled PET tracers were obtained in 9%−85% RCYs. In terms of ^{18}F-labeled TSPO PET tracers, S_N2 displacement was often employed, sometimes with radioactive prosthetic group (*i.e.*, $BrCH_2CH_2^{18}F$ and $^{18}F-FCH_2I$). By now, only two TSPO PET tracers were reported with C_{sp2}-^{18}F motif, in which spirocyclic iodonium ylide method was employed[81]. The radiofluorination yields were comparable with ^{11}C labeling. All TSPO PET tracers possessed good molar activities (Am, >1 Ci/μmol), which was an essential requirement for brain imaging.

3.1. The first TSPO PET tracer

The prototypical PET tracer for TSPO was 1-(2-chlorophenyl)-*N*-[^{11}C]methyl-*N*-(1-methylpropyl)-3-isoquinolinecarboxamide ([^{11}C]PK11195 [^{11}C]**1**), developed more than 2 decades ago. PK11195 was the first non-benzodiazepine-type compound that was a selective antagonist for TSPO. It is an isoquinoline carboxamide discovered and named by a French company, Pharmuka, in 1984[82]. [^{11}C]**1** was initially used as a racemate with high

affinity (inhibition constant [K_i] = 9.3 nmol/L) in rat and selectivity to TSPO[83]. However, further studies in rats suggested that the *R*-enantiomer ([^{11}C](*R*)**1**) binds with a 2-fold greater affinity than the corresponding *S*-enantiomer[84]. The binding affinity of [^{11}C](*R*)**1** is 3.5−4.5 nmol/L in rhesus and 2.1−28.5 nmol/L in human[85]. [^{11}C]**1** has high lipophilicity (log*D* = 3.97), which likely results in high levels of non-specific binding and relatively poor specific binding. For example, the ratio of specific to nonspecific binding of [^{11}C](*R*)**1** in human brain was determined to be only about 0.2−0.5[86]. As the first PET tracer for TSPO [^{11}C]**1** has several disadvantages including a short half-life (20 min), relatively low brain uptake, a poor metabolic profile, and high levels of nonspecific binding resulting in a low SNR, all of which severely limit its widespread clinical use.

Parbo et al.[87] demonstrated that BP of [^{11}C](*R*)**1** and the level of amyloid load in AD patients were positively correlated at a voxel level within the frontal, parietal and temporal cortices [^{11}C](*R*)**1** PET imaging also indicated that cortical distribution of increased inflammation overlapped with amyloid deposition in a multitude of amyloid positive mild cognitive impairment (MCI) patients. In another study, Fan et al.[88] further found that there was significant correlation between increased [^{11}C](*R*)**1** BP and reduced glucose metabolism in AD, MCI, and PD dementia (PDD) subjects. Cortical BP of [^{11}C](*R*)**1** were negatively associated with mini-mental state examination (MMSE) in both AD and PDD patients. Kübler et al.[89] also suggested that the BP of [^{11}C](*R*)**1** was significantly increased within the subregions of the caudate nucleus, putamen, pallidum, precentral gyrus, orbitofrontal cortex, presubgenual anterior cingulate cortex, and the superior parietal gyrus in patients with the parkinsonian phenotype of multiple system atrophy (MSA) compared with healthy controls. Passamonti etal.[90] found that in progressive supranuclear palsy (PSP) patients, the BP of [^{11}C](*R*)**1** within the subregions of thalamus, putamen, and pallidum were significantly elevated compared with controls. They also indicated that in AD patients, BP of [^{11}C](*R*)**1** in the cuneus/precuneus associated with episodic memory impairment, while in PSP patients [^{11}C](*R*)**1** binding within the subregions of the pallidum, midbrain, and pons associated with disease severity. In another study, Gerhard et al.[91] demonstrated that the BP of [^{11}C](*R*)**1** within the subregions of the caudate nucleus, putamen, substantia nigra, pons, pre- and post-central gyrus, and the frontal lobe was significantly increased in corticobasal degeneration (CBD) patients compared to the healthy controls, which may help to characterize the underlying disease activity in CBD patients. Cagnin et al.[92] further suggested that the increased BP of [^{11}C](*R*)**1** in frontotemporal dementia (FTD) patients was mainly presented in the typically affected frontotemporal brain regions, which indicated that the presence of microglial activation reflecting progressive neuronal degeneration. Iannaccone et al.[93] further studied [^{11}C](*R*)**1** PET imaging in Lewy body dementias(DLB) patients. They found that the increased BP of [^{11}C](*R*)**1** in DLB and PD patients was mainly presented in the substantia nigra and putamen. Moreover, substantial additional microglia activation in several associative cortices was found in the patients with DLB.

3.2. *TSPO PET tracers with improved binding specificity and brain uptake*

Due to the above-mentioned limitations of [^{11}C]**1**, development of novel radioligands with greater binding specificity and higher brain uptake was pursued. More than 50 novel PET tracers for TSPO have been reported, including [^{11}C]PBR28 [^{11}C]DAA1106 [^{11}C]DPA713 [^{11}C]vinpocetine [^{11}C]DAC [^{18}F]PBR06 [^{18}F]DPA-714 [^{18}F]PBR111 [^{18}F]FEPPA, and others[94−102] (Fig. 2). In preclinical and early clinical studies, many of these radioligands have been shown to bind to TSPO with improved bioavailability and SNR, lower nonspecific binding, and higher non-displaceable binding potential (BP_{ND}) than [^{11}C]**1**. Other recent reviews have summarized the development of these radioligands[103,104]. Here we will focus on the radioligand design, radioisotope labeling, pharmacokinetics, and PET imaging performance in neurological diseases.

3.2.1. *Phenoxyarylacetamides*

In 2012, Wang et al.[105] reported the automatic radiosynthesis and evaluation of a potent and selective TSPO radioligand, *N*-(2,5-dimethoxybenzyl)-*N*-(5-fluoro-2-phenoxyphenyl)acetamide ([^{11}C]DAA1106 [^{11}C]**2**, Fig. 2), derived from a novel class of phenoxyarylacetamide with high affinity and specificity for TSPO[106]. The binding affinity (K_i) of [^{11}C]2 toward TSPO was 0.043 nmol/L in rat brain and 0.188 nmol/L in monkey brain[107]. [^{3}H]DAA1106 dissociation constant (K_D) were 5- to 6-fold lower than [^{3}H](*R*)-PK11195 in different rat brain regions. Because binding affinity is negatively correlated to the K_D, these data demonstrate that [^{3}H]DAA1106 has higher affinity for TSPO than [^{3}H](*R*)-PK11195[106]. [^{11}C]**2** also has a reasonable lipophilicity (log*D* = 3.65), which could partially contribute to its good BBB penetration. In mice, high [^{11}C]**2** uptake was observed in the brain during scanning (2.1%−3.5% ID/g), about 1.5−2 fold higher than [^{3}H]PK11195. The highest uptake of [^{11}C]**2** was observed in the olfactory bulb [4.2% ID/g at 30 min post-injection (p.i.)], and is commensurate with the highest density of TSPO in the mouse brain, as well as in the cerebellum (3.5% ID/g at 30 min p.i.). Moreover, additional studies demonstrated that [^{11}C]**2** TSPO binding was specific by pre-treatment with DAA1106 and PK11195 prior to *in vivo* imaging with [^{11}C]**2** in both healthy mice and in kainic acid (KA)-lesioned rats[107,108]. Zhang et al.[109] found that [^{11}C]**2** plasma radio-metabolites are much more polar than [^{11}C]**2** and may not cross the BBB in mice [^{11}C]**2** has been widely studied in conditions associated with neuroinflammation. For example, comparing with [^{11}C](*R*)**1** [^{11}C]**2** showed greater retention period at the region of injury in rats with traumatic brain injury (TBI) as evaluated by *in vitro* autoradiography[110]. These results showed that [^{11}C]**2** binds to TSPO with higher affinity, indicating that [^{11}C]**2** may be a better ligand than [^{11}C](*R*)**1** for *in vivo* PET imaging of TSPO in TBI.

In 2009, Gulyás et al.[111] used [^{11}C]**2** for *in vitro* autoradiography studies of human postmortem brain slices obtained from AD patients and age-matched controls. They found that specific binding was significantly higher in the hippocampus, the temporal and parietal cortices, the basal ganglia, and the thalamus of AD brains, suggesting that [^{11}C]**2** can effectively label activated microglia with upregulated TSPO in AD[111]. In another study, mean BP was significantly increased in all measured regions, including the dorsal and medial prefrontal cortices, lateral temporal cortex, parietal cortex, occipital cortex, anterior cingulate cortex, striatum, and cerebellum, as compared to healthy controls[112]. [^{11}C]**2** was used to measure an increase in TSPO binding in the brains of AD patients at a relatively early stage, suggesting widespread upregulation of TSPO even in early AD and further supporting the superiority of [^{11}C]**2** over [^{11}C]**1**. Unfortunately, the study did not directly compare [^{11}C]**2** and [^{11}C]**1** in the same subjects[112]. Similarly, Yasuno et al.[113] demonstrated that [^{11}C]**2**

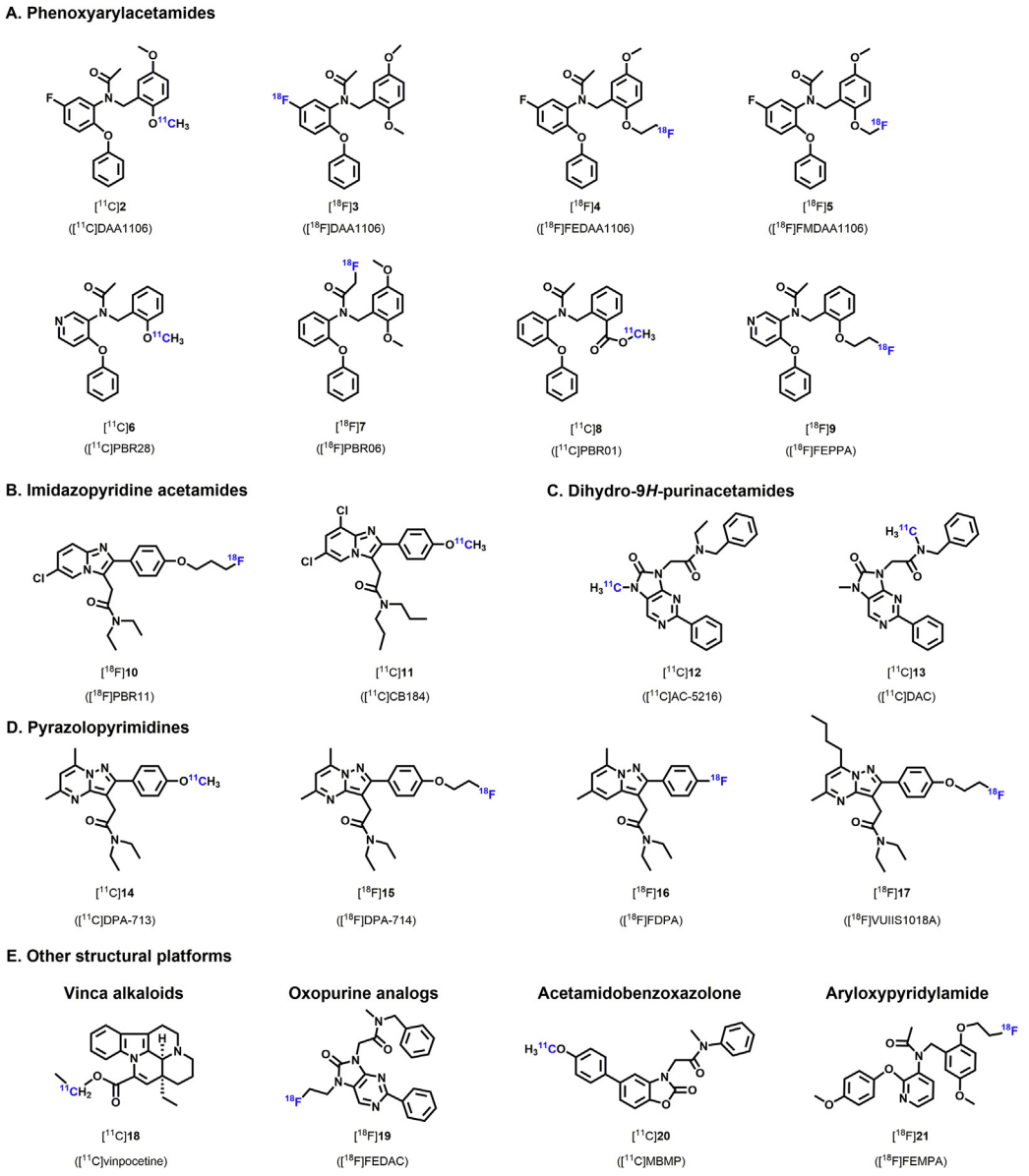

Figure 2 TSPO radioligands with novel chemical structures.

binding to TSPO was also markedly increased throughout many brain regions in MCI subjects compared with healthy controls. There was no significant difference in BP between MCI and AD patients. The high [^{11}C]**2** binding in MCI patients suggested that microglial activation may occur before the onset of clinical dementia symptoms. Further studies are needed to verify this finding.

The chemical composition of DAA1106 includes a fluorine atom. Since ^{18}F has several favorable properties such as a relatively longer half-life (109.7 min) as well as an excellent decay profile (97% β^+ emission) and positron energy (650 keV), labeling DAA1106 with ^{18}F seems to be a logical step for developing a superior TSPO radioligand for PET imaging [^{18}F]**3** showed a very high affinity for TSPO in rat brain[105]. Subsequent [^{18}F]**3** biodistribution studies found low radioactivity uptake in bone without serious defluorination in mice. Furthermore, greater than 96% of the total radioactivity in the mouse brain at 60 min after radioligand injection was found to be unmetabolized radioactivity, attributed to parent [^{18}F]**3**. High [^{18}F]**3** uptake during PET imaging (1.9 ± 0.3% ID/g) was observed in ischemic areas of rat brains as compared to the contralateral side. Additionally, pretreatment with PK11195 demonstrated that [^{18}F]**3** had higher TSPO specificity in the ischemic brains[114].

FEDAA1106(*N*-(5-fluoro-2-phenoxyphenyl)-*N*-(2-(2-fluoroethoxy)-5-methoxybenzyl) acetamide) is a fluorinated ethyl analogue derivative of DAA1106. Recently [^{18}F]FEDAA1106 ([^{18}F]**4**, Fig. 2) has been investigated as a potential radioligand to visualize TSPO *in vivo* using PET imaging. The binding affinity (K_i) of [^{18}F]**4** toward TSPO in rat brain slices was 0.078 nmol/L, and the lipophilicity (log$D$ = 3.81) was higher than [^{11}C](*R*)**1** (log$D$ = 2.78)[115]. Further studies demonstrated high [^{18}F]**4** uptake (2.2%−4.9% ID/g) in the mouse brain, about 1.3−1.6-fold higher than [^{11}C]**2** and 2–3-fold higher than [^{11}C](*R*)**1**[116]. The [^{18}F]**4** uptake in bone was very low (0.31% dose/g at 30 min

p.i. and 0.09% dose/g at 120 min p.i.), which indicated desired stability of the fluoroethyl group against defluorination *in vivo*. Additional PET studies in monkey indicated a high activity attributed to [^{18}F]**4** in the occipital cortex 2 min after injection that remained at nearly the same level during the entire PET measurement (180 min). This was 1.5 times higher than [^{11}C]**2** and 6 times higher than [^{11}C](*R*)**1** (at 30 min p.i.). Additionally, pretreatment with PK11195 showed that the [^{18}F]**4** binding in the occipital cortex was specific. Radiometabolite analyses found that only [^{18}F]**4** was detected in monkey brain homogenates with no evidence of any radioactive metabolites (at 60 min p.i.). The [^{18}F]**4** metabolite profile was similar to [^{11}C]**2** *in vivo*. Another analogue of DAA1106 [^{18}F]FMDAA1106 ([^{18}F]**5**, Fig. 2) was also synthesized and evaluated. The affinity of [^{18}F]**5** for TSPO was found to be similar to [^{11}C]**2**. However [^{18}F]**5** displayed high uptake in bone in mice and monkey, indicating that this radioligand was unstable for *in vivo* defluorination and not a useful PET radioligand[116].

Recently [^{18}F]**4** PET imaging has been used to investigate neurological diseases associated with neuroinflammation[117]. Varrone et al.[118] demonstrated that the distribution volume (V_T) and BP of [^{18}F]**4** in brains was not significantly different in AD and healthy controls. These data suggested that TSPO imaging with [^{18}F]**4** was not a viable tool for monitoring microglial activation in AD. Similarly, another study found no significant differences in the BP_{ND} or V_T values between MS patients and controls, demonstrating that [^{18}F]**4** could not be used to monitor MS brain lesion sites[119]. We speculate that the negative results from the above studies are likely due to the high nonspecific binding of [^{18}F]**4**, as well as genetic variability in TSPO binding in human brains.

PBR28, an analog of DAA1106, is a promising second-generation TSPO radioligand [^{11}C]PBR28 ([^{11}C]**6**, Fig. 2, *N*-(2-[^{11}C]methoxybenzyl)-*N*-(4-phenoxypyridin-3-yl)acetamide) was originally developed by Pike and colleagues[120,121] [^{11}C]**6** showed a high affinity for TSPO in rat (K_i = 0.680 ± 0.027 nmol/L), monkey (K_i = 0.944 ± 0.101 nmol/L), and human (K_i = 2.47 ± 0.39 nmol/L) mitochondria [^{11}C]**6** also displayed high lipophilicity (log*D* = 3.01 ± 0.11)[120] and was very stable; 99.8% was unchanged after incubation with rat brain homogenate in saline for 2 h at 37 °C. The radioactivity of this radioligand was rapidly detected in monkey brain, with peak uptake occurring in all examined TSPO-containing regions at 10 min p.i., and then was quickly washed out to a low level. Maximal uptake was 394% standard uptake volume (SUV) in the choroid plexus of the fourth ventricle[120]. They also found that [^{11}C]**6** radioactivity in all examined regions was rapidly and substantially reduced in monkey brain after administration of PK11195, indicating that [^{11}C]**6** binding to TSPO was specific. The specific binding of this ligand was greater than 90% of its total uptake in monkey brain[121]. Another study demonstrated that the specific binding of [^{11}C]**6** in monkey cerebellum was about 80-fold higher than [^{11}C]**(R)1**[122].

Brown et al.[123] further suggested that [^{11}C]**6** would cause relatively modest radiation burden in humans, similar to several other ^{11}C-radioligands used for brain imaging [^{11}C]**6** has been used as a radioligand to study several neurological diseases associated with neuroinflammation. Oh et al.[124] reported [^{11}C]**6** PET scans from 11 subjects with MS and 7 healthy volunteers. They found that [^{11}C]**6** uptake was significantly increased in focal regions of active inflammation, as proven by gadolinium contrast enhancement, in comparison to the contralateral normal-appearing white matter. Furthermore, the increase in [^{11}C]**6** uptake exceeded the appearance of contrast enhancement in MRI of some inflammatory lesions, indicating the important role of early glial activation in MS lesion formation and further confirming that TSPO is an informative biomarker of glial activation or neuroinflammation in MS. Global [^{11}C]**6** binding was correlated with disease duration, but not with clinical disability. However, the sample size was relatively small, limiting the translation of these data[124]. Subsequently, Hirvonen et al.[125] also performed [^{11}C]**6** imaging in patients with unilateral temporal lobe epilepsy (TLE). Their study demonstrated that [^{11}C]**6** uptake in TLE patients was higher ipsilateral to the seizure focus, which consisted of the hippocampus, parahippocampal gyrus, amygdala, fusiform gyrus, and choroid plexus, indicating increased TSPO expression. Further, this asymmetry was more obvious in patients with hippocampal sclerosis. However, a larger sample size is needed to determine the generalizability of these results across different types of epilepsy[125]. In another study, Gershen et al.[29] found that, compared to controls [^{11}C]**6** binding in patients with TLE was significantly elevated in both ipsilateral temporal regions and contralateral regions to seizure foci (including hippocampus, amygdala, and temporal pole), suggesting increased TSPO extending beyond the seizure focus and involving both temporal lobes and extratemporal regions. This demonstrated that anti-inflammatory therapy may be important in treating drug-resistant epilepsy. In 2013, Kreisl et al.[59] found that [^{11}C]**6** binding in patients with AD, but not those with MCI, was significantly higher than controls in cortical brain regions, especially in the parietal and temporal cortices [^{11}C]**6** binding inversely correlated with performance in a cognitive function assessment. They demonstrated that neuroinflammation, as defined by elevated [^{11}C]**6** binding to TSPO, occurs after conversion of MCI to AD and exacerbates with disease progression. However [^{11}C]**6** PET imaging in humans is limited due to TSPO binding affinity differences related to genotype[59]. In another study, Lyoo et al.[126] used an absolute quantitation method (V_T/f_P, plasma free fraction of radioligands (f_P)) to confirm that [^{11}C]**6** binding was greater in AD patients than healthy controls in temporo-parietal regions, but not in the cerebellum. The authors then explored the use of the cerebellum as a pseudo-reference region and determined the standard uptake volume ratio (SUVR). SUVR demonstrated greater TSPO binding than absolute quantification and identified one additional TSPO upregulated region, indicating that SUVR analysis may have greater sensitivity. This new analysis needs to be replicated in more AD patients before being widely implemented. In 2016, Kreisl et al.[127] examined AD clinical progression and demonstrated that the annual rate of elevated [^{11}C]**6** binding in temporo-parietal regions was about 5-fold higher in AD with clinical progression than in patients without progress. They suggested that TSPO may be used as a marker of Alzheimer's progression and response to anti-inflammatory therapies. Since this study had a small sample size the authors subsequently studied TSPO PET imaging in different clinical subtypes of AD, including posterior cortical atrophy (PCA) and amnestic AD[128]. They found that [^{11}C]**6** binding in occipital, posterior parietal, and temporal regions was significantly increased in PCA patients compared with controls. However, in amnestic AD patients [^{11}C]**6** binding in inferior and medial temporal cortex was much greater than controls. They suggested that neuroinflammation is also closely correlated with neurodegeneration across different subtypes of AD. However, this study was limited by its relatively low sample size and variability in TSPO binding affinity across subjects.

Recently, TSPO imaging has also been used to investigate other neurodegenerative diseases. For example, Lois et al.[129] used [^{11}C]**6** PET/MR imaging to study neuroinflammation in Huntington's disease (HD). They reported that [^{11}C]**6** binding in the putamen and pallidum was significantly increased in HD patients compared to controls. They also observed that TSPO binding was significantly elevated in the basal ganglia of pre-symptomatic subjects, indicating that neuroinflammation is an early pathological process correlated with subclinical progression of HD. Further, they showed that, in some HD patients, TSPO binding was greater in thalamic subnuclei and brainstem regions associated with visual function, motor function, and motor coordination. The authors assert that [^{11}C]**6** PET/MR imaging provides a high signal-to-background ratio and has the potential for clinical evaluation of HD progression, albeit the study had a relatively small sample size[129]. Other work demonstrated that patients with ALS had greater [^{11}C]**6** binding in the precentral gyrus compared to controls[130,131]. Subsequently, Ratai et al.[132] used integrated imaging technologies and found that increased [^{11}C]**6** binding in response to glial activation in the precentral gyrus in patients with ALS was co-localized and related to neuronal injury/loss, as monitored by decreased *N*-acetylaspartate/creatine (NAA/Cr).

Another 2nd-generation TSPO ligand, PBR06, was labeled with ^{18}F, ^{18}F-*N*-fluoroacetyl-*N*-(2,5-dimethoxybenzyl)-2-phenoxyaniline ([^{18}F]PBR06 [^{18}F]**7**, Fig. 2). The half-life of ^{18}F allows for a longer data acquisition period, and may be required to match the pharmacokinetics of the elevated binding density. The binding affinity (K_i) of [^{18}F]**7** toward TSPO was 0.30 ± 0.08 nmol/L in monkey brain mitochondrial homogenates and 1.0 nmol/L in human brain tissue [^{18}F]**7** also has a very high lipophilicity (log$D$ = 4.01), greater than [^{11}C]**6**. Elevated lipophilicity may improve BBB penetration, but also tends to increase nonspecific binding in the brain. However [^{18}F]**7** and [^{11}C]**6** have very similar brain uptake, when corrected by V_T/f_P[133]. [^{18}F]**7** radioactivity was observed in monkey brains with peak uptake occurring in examined TSPO-containing sites at 27 and 72 min after injection. Maximal binding was 371 ± 89% SUV and occurred in the choroid plexus of the fourth ventricle. Subsequently, the radioactivity slowly washed out [^{18}F]**7** also showed no obvious evidence of *in vivo* defluorination. The radioactivity of unchanged [^{18}F]**7** in the brain was very high (>90%) at 30 min p.i. Moreover, the radiometabolites were more hydrophilic than [^{18}F]**7**. This study also demonstrated that [^{18}F]**7** had a very low ratio of TSPO-nonspecific to specific binding in monkey[134]. [^{18}F]**7** has also been widely studied in many neurological disease models. Lartey et al.[135] found that after stroke [^{18}F]**7** accumulation in mouse brain peaked at 5 min p.i., then decreased gradually, remaining significantly higher in infarct regions than in noninfarct sites. Pre-treatment with PK11195 eliminated the difference in [^{18}F]**7** binding between infarct and noninfarct regions. This study demonstrated that TSPO is a potential biomarker of neuroinflammation in mouse stroke models. However, further research in monkeys and humans is needed. In another study, James et al.[136] found that [^{18}F]**7** binding in 15- to 16-month-old APP$^{L/S}$ mice was much higher in the cortex and hippocampus compared with age-matched wild-types and was well correlated with autoradiography and immunostaining results. The authors suggested that [^{18}F]**7** could be a viable biomarker for monitoring TSPO/microglia throughout AD progression and treatment, however, these data need to be replicated in higher species. Subsequently, Simmons et al.[137] found that [^{18}F]**7** could monitor microglial activation in the cortex, striatum, and hippocampus of R6/2 mice treated by vehicle at a late stage of HD and in BACHD mice at an early mid-stage of symptomatic HD. In both HD mouse models [^{18}F]**7** binding could reflect the inhibitory effects of LM11A-31, a *P*75^{NTR} ligand known to reduce neuroinflammation. Thus [^{18}F]**7** is also a potential radiotracer of therapeutic efficacy in HD mice.

Fujimura et al.[138] further quantified TSPO using [^{18}F]**7** in healthy human brains. They showed that [^{18}F]**7** binding could be used to measure TSPO in human brains using 120 min of image acquisition. Although brain radioactivity signal is likely from a mix of radiometabolites, the radio signal of contamination is also very low (<10%). Moreover, Fujimura et al.[139] reported that [^{18}F]**7** radioactivity in human bone was very low. The effective dose of [^{18}F]**7** was 18.5 μSv/MBq in human subjects, a moderate dose compared to other ^{18}F radioligands. In another study, Singhal et al.[100] found that [^{18}F]**7** and [^{11}C]**6** correlated with white matter, but not lesion sites, in MS patients. Their results also demonstrated that, compared with [^{11}C]**6**, MS-correlated lesional changes detected using [^{18}F]**7** had higher clinical relevance; however, their sample size was relatively small.

Both [^{11}C]PBR01 ([methyl-^{11}C]methyl 2-((*N*-(2-phenoxyphenyl)-acetamido)-methyl)benzoate [^{11}C]**8**, Fig. 2), and [^{18}F]**7** are aryloxyanilide compounds [^{11}C]**8** has also been evaluated in monkeys as a potential TSPO radioligand[134]. The binding affinity (K_i) of [^{11}C]**8** toward TSPO in monkey brain mitochondrial homogenates was 0.24 ± 0.04 nmol/L, similar to [^{18}F]**7**. Both radioligands show high brain uptake. Further, pre-block with PK11195 of both [^{18}F]**7** and [^{11}C]**8** before PET imaging caused rapid washout of radioactivity in monkey brain, suggesting that binding was highly specific. In fact, both radioligands showed similar clearance, time to peak uptake, and washout rates. However [^{18}F]**7** may have greater potential for use in human subjects, as demonstrated by brain radioactivity quantified with standard compartmental models and a higher specific binding.

[^{18}F]FEPPA (*N*-acetyl-*N*-(2-[^{18}F]fluoroethoxybenzyl)-2-phenoxy-5-pyridinamine [^{18}F]**9**, Fig. 2), is a novel ^{18}F-radiolabelled phenoxyanilide, the fluoroethoxy analogue of PBR28. FEPPA had a very high binding affinity (K_i = 0.07 nmol/L) for the PBR in rat mitochondrial membrane preparations and displayed a suitable lipophilicity (log$P$ = 2.99). Wilson et al.[79] demonstrated that [^{18}F]**9** uptake in rat brain was moderate (SUV 0.6) at 5 min p.i. and slowly washed out (SUV 0.35) at 60 min p.i. The highest radioactivity in rat brain was observed in the hypothalamus and olfactory bulb [^{18}F]**9** was quickly metabolized, but no lipophilic metabolites were present and only 5% radiometabolites were observed in the brain. There was some limitation with the blocking studies to assess specific binding of [^{18}F]**9** in rat brain due to elevation of circulating radioligands and the lack of a reference region, however the ratio of tissue to plasma was reduced by approximately 97% with administration of cold PBR28[79].

[^{18}F]**9** was tested *in vivo* in humans and applied to investigate several neuropsychiatric diseases[140]. Suridjan et al.[141] found that [^{18}F]**9** binding was significantly greater in AD patients compared to healthy controls in grey matter areas, including the hippocampus, and the prefrontal, temporal, parietal, and occipital cortices [^{18}F]**9** binding was also increased in white matter of AD patients, including the posterior limb of the internal capsule and the cingulum bundle[141]. Setiawan et al.[30] reported elevated TSPO V_T during major depressive episodes in the grey matter regions, including the prefrontal and anterior cingulate cortex, a finding replicated with [^{18}F]**9** [^{11}C]**6** and [^{11}C](*R*)**1** in subsequent studies[142–146]. Attwells et al.[75] reported elevated TSPO V_T in OCD, particularly in the cortico-striatal-thalamic circuit involving the orbitofrontal cortex. Ghadery et al.[94] did not observe activated microglia in gray or white matter using [^{18}F]**9** PET imaging in PD although additional studies are required to determine the utility of [^{18}F]**9** as a radiotracer of microglial activation in neurodegenerative diseases.

3.2.2. Imidazopyridine acetamides

PBR111(2-(6-chloro-2-(4-(3-fluoropropoxy)phenyl)imidazo[1,2-*a*]pyridin-3-yl)-*N*,*N*-diethylacetamide) is a metabolically stable imidazo pyridineacetamide derivative with high binding affinity and selectivity for TSPO[147]. [^{18}F]PBR111 ([^{18}F]**10**, Fig. 2) is a potential TSPO radioligand (K_i = 3.7 ± 0.4 nmol/L) and has an appropriate lipophilicity (log*P* = 3.2 ± 0.1). The highest [^{18}F]**10** uptake was 0.2%−0.3% ID/g in rat brain at 15 min p.i., which then rapidly washed out. However [^{18}F]**10** uptake in femur was 0.6% and 2.2% ID/g at 15 min and 4 h p.i., respectively, indicating that it may be unstable and defluorinated *in vivo*. Metabolic analysis demonstrated that, in the rat cortex, 55%−80% of the radioactivity represented [^{18}F]**10** at 15 min p.i., which further decreased to 30% at 4 h p.i.[148]. Moreover, Van Camp et al.[149] used *in vitro* autoradiography and found that [^{18}F]**10** binding was significantly increased in α-amino-3-hydroxy-5-methyl-4-isoxazole propionic acid (AMPA)-lesioned areas in rat brain compared to the control side. Moreover, blockade with an excess of unlabeled PK11195 or PBR111 significantly inhibited binding in the lesioned area. They also observed higher [^{18}F]**10** uptake in AMPA-lesioned rat brains than [^{11}C]**1** uptake using *in vivo* PET imaging. Unlabeled PK11195 or PBR111 quickly and fully displaced the radiolabel. However, further preclinical and clinical studies using [^{18}F]**10** as a radiotracer of neuroinflammation are needed. Subsequently, Guo et al.[150] further investigated [^{18}F]**10** in human subjects. Using a 2-tissue compartment model, they concluded that [^{18}F]**10** has a high specific binding for TSPO in the healthy human brain *in vivo*.

[^{11}C]CB184(*N*,*N*-di-*n*-propyl-2-[2-(4-[^{11}C]methoxyphenyl)-6,8-dichloroimidazol[1,2-*a*]pyridine-3-yl] acetamide [^{11}C]**11**, Fig. 2), is a new and improved alternative to [^{11}C](*R*)**1**. The binding affinity (K_i) of [^{11}C]**11** toward TSPO was 0.54 nmol/L, as measured in an *in vitro* binding study, and lower lipophilicity (log*P* = 2.06 ± 0.02) compared to [^{11}C](*R*)**1** (log*D* = 2.78)[151]. The highest [^{11}C]**11** uptake in mouse brain is observed in the olfactory bulb (1.45 ± 0.03% ID/g), cerebellum (1.384 ± 0.091% ID/g), hippocampus (1.225 ± 0.067% ID/g), and pons (1.045 ± 0.102% ID/g) [^{11}C]**11** uptake in mouse brain was monitored at 30 min p.i., and the uptake levels were nearly stable from 30 to 60 min p.i. After pre-administration with PK11195, the [^{11}C]**11** uptake level was significantly reduced relative to controls in every brain region, indicating that [^{11}C]**11** binding specificity is very high in mouse brain tissue. Metabolic analyses demonstrated that the percentages of unchanged parent compound for [^{11}C]**11** were 92.7 ± 5.8% in the brain and 36.2 ± 15.5% in the plasma at 30 min p.i.[151]. Moreover, Vállez Garciaet al.[152] evaluated [^{11}C]**11** labeling in neuroinflammation. Their study showed greater [^{11}C]**11** uptake in the amygdala, olfactory bulb, medulla, pons, and striatum in herpes simplex encephalitis (HSE) rats compared to controls. Similarly, the BP of [^{11}C]**11** in HSE rats was significantly higher ($P < 0.05$) in the amygdala, hypothalamus, medulla, pons, and septum compared with control rats. Their results indicate that [^{11}C]**11** is a good alternative radioligand for TSPO PET imaging. However, more studies are need to determine the utility of [^{11}C]**11** PET imaging for detection of neuroinflammation in non-human primates and humans.

Subsequently, Toyohara et al.[153] found that [^{11}C]**11** PET imaging in healthy humans showed quick uptake in the brain followed by rapid clearance during a 90-min dynamic scan [^{11}C]**11** was equally distributed in the gray matter and was greatest in the thalamus, followed closely by the cerebellar cortex and elsewhere. Regional differences in [^{11}C]**11** binding were small, but the observed [^{11}C]**11** binding pattern was in agreement with the TSPO distribution in normal human brain. The effective dose of [^{11}C]**11** was 5.9 ± 0.6 μSv/MBq in human subjects[154].

3.2.3. Dihydro-9H-purinacetamides

AC-5216 (*N*-benzyl-*N*-ethyl-2-(7-methyl-8-oxo-2-phenyl-7,8-dihydro-9*H*-purin-9-yl)acetamide) is an oxopurine labeled with ^{11}C, and is another new candidate TSPO PET tracer ([^{11}C]**12**, Fig. 2)[155]. The binding affinity (K_i) of [^{11}C]**12** toward TSPO was 0.297 nmol/L in whole rat brain and the lipophilicity was appropriate (log$D_{7.4}$ = 3.3)[156]. Moreover, the TSPO binding site for AC-5216 may be more similar to PK11195 than to other TSPO ligands. The radioligand was observed to promote BBB penetration and enter mouse brain regions at 1 min p.i. In the olfactory bulb and cerebellum [^{11}C]**12** radioactivity was greater than 1.3% ID/g at 5 min p.i. The absorption level peaked at 15 min p.i. and then decreased until 60 min p.i. The greatest uptake of [^{11}C]**12** was present in the olfactory bulb (2.5% ID/g at 15 min p.i.), and moderate uptake was observed in the cerebellum (1.5% ID/g at 15 min p.i.). Uptake in the occipital cortex of monkey brain was greater than in other brain structures such as the cerebellum, frontal cortex, striatum, and thalamus. Pre-block with AC-5216 or PK11195 could inhibit the maximum uptake of [^{11}C]**12** to 30%−40% of the control uptake, indicating specific binding in the monkey brain *in vivo* [^{11}C]**12** radioactivity was also measured in mouse brain homogenate as a minor (<10%) radiometabolite at 60 min p.i.

Subsequently, Yanamoto et al.[157] used [^{11}C]**12** as a novel TSPO radioligand in a KA-induced neuroinflammatory rat model. They used *in vitro* and *ex vivo* autoradiography to demonstrate that [^{11}C]**12** radioactivity was significantly elevated in the striatum lesions induced by KA (2- to 3-fold higher than the contralateral striatum). Pre-block with AC-5216 or PK11195 abolished the difference in [^{11}C]**12** uptake levels between the lesioned and nonlesioned sides, suggesting that [^{11}C]**12** has very high specificity for TSPO[157]. However [^{11}C]**12** needs to be further studied in preclinical and clinical trials of many other neuroinflammatory neurological diseases to determine if it is a viable alternative TSPO radioligand.

DAC is a novel derivative of AC-5216 that can be labeled with ^{11}C by reacting a desmethyl precursor with [^{11}C]CH_3I. The binding affinity for [^{11}C]DAC ([^{11}C]**13**, Fig. 2, K_i = 0.23 ± 0.02 nmol/L) is similar to [^{11}C]**12** in rat, however, it has lower lipophilicity (log*D* = 3.0) compared with [^{11}C]**12**, indicating that [^{11}C]**13** may have higher specificity and faster kinetics[158]. The greatest observed [^{11}C]**13** uptake was 2.24 ± 0.16% ID/g at 1 min p.i. in mouse brain, followed by rapid clearance. Low levels of radiometabolites of [^{11}C]**13** were detected in the mouse brain (<5%) at 60 min p.i. Yanamoto et al.[158] demonstrated that [^{11}C]**13** binding in KA-lesioned rats was greater in the lesioned striatum compared to control striatum *in vivo*, similar to [^{11}C]**12**. Pre-block with DAC or PK11195 significantly decreased [^{11}C]**13** uptake in the lesioned striatum to levels similar to the control side. Moreover [^{11}C]**13** TSPO binding was 1.8-fold higher in the lesioned striatum than in the contralateral striatum, as measured by *in vitro* autoradiography. In another study, Yui et al.[99] reported that early infarction with a slight TSPO expression elevation in ischemic rat brains could be measured with [^{11}C]**13** PET imaging with very high molar activity (average 4060 GBq/μmol). However, binding was not observed with low molar activity of [^{11}C]**13** (37 GBq/μmol), which is consistent with the *in vitro* autoradiography results. However, neuroinflammation could be observed in the rat brain 4 days after

ischemia using specific activity (SA) [^{11}C]**13**. Pre-block with AC-5216 or PK11195 diminished the difference in radioactivity between the ipsilateral and contralateral sides, suggesting that the increased radioactivity in the infracted regions was specific to TSPO[99]. However [^{11}C]**13** imaging for TSPO needs to be confirmed in preclinical and clinical studies.

3.2.4. *Pyrazolopyrimidines*

N,*N*-Diethyl-2-[2-(4-methoxyphenyl)-5,7-dimethyl-pyrazolo[1,5-*a*]pyrimidin-3-yl]-acetamide (DPA-713) is a novel pyrazolopyrimidine ligand for TSPO. DPA-713 labeling with ^{11}C can be performed by *O*-alkylation of a phenolic derivative (*N*,*N*-diethyl-2-[2-(4-hydroxyphenyl)-5,7-dimethyl-pyrazolo[1,5-*a*]pyrimidin-3-yl]acetamide) with [^{11}C]CH_3I to produce [^{11}C]DPA-713 ([^{11}C]**14**, Fig. 2). The radioligand displayed high affinity in rat (K_i = 4.7 nmol/L), mouse (K_i = 1.3 nmol/L), and human (K_i = 15.0−66.4 nmol/L)[85,159] [^{11}C]**14** also has high lipophilicity (log$D$ = 2.4). In *Papio anubis* baboon brains [^{11}C]**14** radioactivity peaked at 20 min and remained constant during scanning. Pre-injection with PK11195 (5 mg/kg) successfully decreased the radioactivity by 70% at 60 min throughout the whole brain, indicating that [^{11}C]**14** binding in the baboon was specific for TSPO[160] [^{11}C]**14** has been widely used as a TSPO radioligand to study neuroinflammation. Boutin et al.[161] found that [^{11}C]**14** showed a greater difference between healthy and damaged brain parenchyma compared with [^{11}C]**1** (2.5 ± 0.14- *vs.* 1.6 ± 0.05-fold increase, respectively) in an AMPA induced model of neuroinflammation in rats [^{11}C]**14** had a better SNR ratio than [^{11}C]**1** due to higher binding specificity[161,162]. Chaney et al.[163] used PET imaging to demonstrate that [^{11}C]**14** uptake was markedly increased in the ipsilateral *versus* contralateral hemispheres in distal middle cerebral artery occlusion (dMCAO) mice. Elevated radioactivity was also measured in the ipsilateral hemisphere of dMCAO when compared with sham mice. Similarly, using *ex vivo* autoradiograph, elevated [^{11}C]**14** radioactivity was observed in infarcted tissue compared to surrounding healthy brain tissue[163]. Recently, Chaney et al.[164] found that [^{11}C]**14** uptake in mice with ischemic stroke was significantly elevated in infarcted brain tissue compared to contralateral brain regions at both acute and chronic time-points. Further, using *in vitro* autoradiography, increased [^{11}C]**14** radioactivity was observed in infarcted *versus* contralateral brain regions. Importantly, microglial activation [determined by CD68 (cluster of differentiation 68) immunostaining] and [^{11}C]**14** PET tracer binding were correlated[164]. Further studies in non-human primates and humans are needed.

Endres et al.[165] first demonstrated that [^{11}C]**14** gives a greater brain signal according to dose-normalized time activity curves, indicating that [^{11}C]**14** is a potential radioligand for evaluating TSPO binding with PET imaging in human subjects. In another study, they found that the distribution of [^{11}C]**14** in human subjects was similar to the known biodistribution of TSPO. Further, dosimetry with [^{11}C]**14** is similar to that of [^{11}C]**6** in humans [^{11}C]**14** also has a similar dose burden compared to other ^{11}C-labeled PET tracers[166]. Recently, Endres et al.[166] demonstrated that selective [^{11}C]**14** binding in healthy human brain was much higher than [^{11}C](*R*)**1**. Subsequently, Gershen et al.[29] found that [^{11}C]**14** radioactivity was greater ipsilateral to seizure foci, as compared to contralateral, in patients with TLE. However, the sample size was relatively small. Although [^{11}C]**14** has good potential as a TSPO radioligand due to its highly specific binding, we have observed an increased V_T over time, consistent with the accumulation of radiometabolites in the human brain[50].

N,*N*-Diethyl-2-(2-(4-(2-fluoroethoxy)phenyl)-5,7-dimethylpyrazolo[1,5-*a*]pyrimidin-3-yl)acetamide (DPA-714) is a novel 2-phenylpyrazolo [1,5-*a*]pyrimidineacetamide that is a specific TSPO ligand. It was designed with a fluorine atom in its chemical structure, allowing for labeling with fluorine-18 [^{18}F]DPA-714 ([^{18}F]**15**, Fig. 2) is a close derivative of [^{11}C]**14**. The affinity of DPA-714 for TSPO ($K_i = 7.0 \pm 0.4$ nmol/L) is lower than DPA-713 in rat. DPA-714 also has a high lipophilicity (log$D$ = 2.44), similar to DPA-713[167]. James et al.[167] evaluated the biodistribution of [^{18}F]**15** in rodents and baboon and found that [^{18}F]**15** uptake in rat bone was very low, indicating this radioligand is stable against defluorination *in vivo*. Similarly [^{18}F]**15** is capable of penetrating the BBB and accumulating in the baboon brain. The binding of [^{18}F]**15** in baboon brain could also be successfully blocked by PK11195, indicating TSPO specific binding. Further [^{18}F]**15** radiometabolites were negligible in rat brain (<3% at 30 min p.i.)[168]. James et al.[167] found that [^{18}F]**15** uptake in a quinolinic acid (QA)-lesioned rat brain model was significantly increased in the ipsilateral striatum and reduced after pre-block with PK11195. In one study, Doorduin et al.[169] compared the radioactivity of [^{18}F]**15** [^{11}C]**14**, and [^{11}C](*R*)**1** in a rat model of herpes encephalitis. They showed that specific uptake of [^{18}F]**15** and [^{11}C]**14** was higher than [^{11}C](*R*)**1** in infected brain areas. Chauveau et al.[162] further directly compared the uptake of [^{18}F]**15** [^{11}C]**14**, and [^{11}C](*R*)**1** in a unilateral, striatal AMPA-lesioned rat model. They reported that [^{18}F]**15** performed better than [^{11}C]**14** and [^{11}C](*R*)**1** due to the greatest ipsilateral to contralateral uptake ratio and the highest BP. Moreover, the ability to label DPA-714 with ^{18}F, the preferred PET isotope, supports its dissemination and clinical use[162]. Thomas et al.[170] demonstrated that [^{18}F]**15** PET signal in a rat model of subarachnoid hemorrhage (SAH) was correlated to the degree of bleeding, suggesting that [^{18}F]**15** PET imaging could be used to improve SAH management in human patients. In another study, Gargiulo et al.[171] used high-resolution PET/CT imaging and reported increased [^{18}F]**15** binding in the brainstem of transgenic SOD1^{G93A} mice, an ALS mouse model. The brainstem is a region known to have significant degeneration and activated microglia in ALS. Thus [^{18}F]**15** might be a suitable marker to evaluate microglial activation in the SOD1^{G93A} mouse model[171] [^{18}F]**15** PET imaging was also investigated in other neurological diseases associated with neuroinflammation. Miyajima et al.[172] monitored [^{18}F]**15** uptake with PET imaging and found that it was markedly increased before selective neuronal loss (SNL) in an ischemic stroke rat model, a change that was also observed by *ex vivo* autoradiography. Tan et al.[173] used [^{18}F]**15** PET/CT imaging to monitor neuroinflammation and evaluate the therapeutic effect of bone marrow stromal cells (BMSC) in an ischemic stroke rat model, indicating that [^{18}F]**15** has highly potential for clinical application. Additionally, Nguyen et al.[174] reported that [^{18}F]**15** binding in a mouse model with mesial TLE peaked on Day 7, which is mostly correlated with microglial activation, whereas reactive astrocytes become the main TSPO expression cells after 14 days. They demonstrated that TSPO has great potential as a longitudinal imaging biomarker and could be used to determine the therapeutic window in epilepsy, as well as to monitor the response to therapy[174].

In healthy human subjects, Arlicot et al.[175] measured the highest cerebral [^{18}F]**15** uptake at 5 min p.i., followed by two decreasing phases: a promoted washout (5−30 min) and then a slower phase. They concluded that [^{18}F]**15** is a potential PET tracer with good *in vivo* stability and biodistribution and an acceptable estimated effective dose[175]. Recently [^{18}F]**15** PET imaging has been widely used to study AD. Golla et al.[176] demonstrated a small but significant difference in [^{18}F]**15** BP_{ND}

between AD patients and healthy subjects; however, the sample size was very small. Subsequently, Hamelin et al.[177] performed [^{18}F]**15** PET imaging in more AD patients. They found that temporo-parietal cortex [^{18}F]**15** uptake was greater in AD patients that were high and mixed affinity binders as compared to controls, particularly at the prodromal stage. Moreover, TSPO binding was related with MMSE scores and grey matter volume, and with Pittsburgh compound B binding[177]. Similarly, Hamelin et al.[101] found that [^{18}F]**15** binding was significantly increased in patients with AD compared to controls both at prodromal and demented stages. They also observed that the change in [^{18}F]**15** uptake over time was positively correlated with three clinical outcome measures (Clinical Dementia Rating, MMSE, hippocampal atrophy), indicating that increased neuroinflammation (compared to the initial PET imaging) was associated with negative clinical AD progression. However, various factors may influence disease progression differently among different patients rather than across disease stages[101]. Subsequently, Hagens et al.[178] further demonstrated that [^{18}F]**15** could be used to monitor increased focal and diffuse neuroinflammation in progressive MS patients, but observed that the differences were most pronounced in high-affinity binders.

N,*N*-Diethyl-2-(2-(4-[^{18}F]fluorophenyl)-5,7-dimethylpyrazolo [1,5-*a*]pyrimidine-3-yl)-acetamide ([^{18}F]FDPA [^{18}F]**16**, Fig. 2), is a fluorine-containing pyrazolopyrimidine and fluoroaryl derivative of [^{18}F]**15** that has a fluorine atom located on the aromatic moiety, and is also a potential PET tracer. FDPA has a higher binding affinity (K_i = 2.0 ± 0.8 nmol/L) than DPA-714, and [^{18}F]**16** also has appropriate lipophilicity (log$D$ = 2.34 ± 0.05)[179]. [^{18}F]**16** uptake in mouse brain was moderate (3.69% ID/g) at 2 min p.i., and the radioactivity washout was also reasonable (1.15% ID/g) at 45 min p.i. Moreover, bone uptake was negligible (<1% ID/g), indicating that little or no defluorination occurred *in vivo* in mice. Wang et al.[179] further studied [^{18}F]**16** PET imaging in neuroinflammation models. Using a rat ischemia model, they demonstrated that maximum [^{18}F]**16** uptake occurred at the ischemic site and reached a peak of 1.20 SUV at 10 min p.i. After pre-treatment with PK11195, the PET signal was significantly reduced by *ca.* 80%, indicating high specificity of [^{18}F]**16** binding *in vivo*. Moreover, they found that [^{18}F]**16** could easily cross the BBB. And in the APP/PS1 mouse mode, they found that [^{18}F]**16** increased to 1.50 ± 0.13 SUV at 3 min p.i., indicating 1.6-fold higher uptake and slow washout compared to age-matched controls. They obtained similar results in ischemic rat brains and APP/PS1 mouse brains using *in vitro* autoradiography[179]. In another study, Keller et al.[180] showed that [^{18}F]**16** radioactivity in APP/PS1 mouse brains was substantially elevated with age using *in vivo* PET imaging and *in vitro* brain autoradiography. They also observed significant differences in binding between wildtype and transgenic animals *in vivo* at 9 months and *ex vivo* at 4.5 months. After pre-block with PK11195 [^{18}F]**16** uptake was significantly decreased in all brain regions studied[180]. PET imaging of [^{18}F]**16** has not yet been translated to higher species.

2-(7-Butyl-2-(4-(2-[^{18}F]fluoroethoxy)phenyl)-5-methylpyrazolo [1,5-*a*]pyrimidin-3-yl)-*N*,*N*-diethy-lacetamide ([^{18}F]VUIIS1018A [^{18}F]**17**, Fig. 2), is a novel analog of [^{18}F]**15** that features a 700-fold higher *in vitro* binding affinity for TSPO than [^{18}F]**15.** [^{18}F]**17** exhibits an exceptional high TSPO binding affinity *in vitro* study (IC_{50} = 16.2 pmol/L)[181]. [^{18}F]**17** has a high lipophilicity (log$D$ = 3.74 ± 0.01), but, unlike [^{18}F]**15**, its lipophilicity is slightly higher than the appropriate range (log$D$ = 1.0−3.5)[78]. The lipophilicity of [^{18}F]**17** needs to be reduced for PET imaging in the brain. Low [^{18}F]**17** radioactivity was observed (<1.0% ID/g) in healthy mouse brains at all time points, which is consistent with the normal TSPO distribution. Low uptake (1.6% ID/g) was also observed in the femur at 1 min p.i., which increased slightly (2.1% ID/g) at 60 min p.i., indicating that there was no significant defluorination *in vivo*. Metabolite analysis showed that 95.7 ± 3.0% and 86.2 ± 2.1% of intact [^{18}F]**17** remained in the brain at 30 and 60 min p.i., respectively, which is greater than the ratio of intact [^{18}F]**15** observed in brain. They further evaluated the radioligand using a focal cerebral ischemic rat model. The results demonstrated that [^{18}F]**17** uptake substantially increased on the ischemic side compared to the contralateral side. After blocking with unlabeled VUIIS1018A and PK11195, the radioactivity on the ischemic side of the brain was markedly decreased. They observed the same trend using *in vitro* autoradiography[78]. No translational imaging data has been reported in primates or humans.

3.2.5. *Vinca alkaloids*

Vinpocetine is a vinca alkaloid compound widely utilized in the prevention and therapy of cerebrovascular disorders. It was developed as a PET tracer labeled with ^{11}C and has good pharmacokinetic characteristics and high affinity to TSPO. Gulyás et al.[182] performed a distribution study of [^{11}C]vinpocetine ([^{11}C]**18**, Fig. 2) in a cynomolgous monkey and showed that [^{11}C]**18** could rapidly enter the brain [^{11}C]**18** radioactivity was heterogeneously distributed among different brain regions and was greatest in the thalamus, the basal ganglia, and certain neocortical regions.

[^{11}C]**18** binds to TSPO in brain tissue with low affinity (IC_{50} = 0.2 μmol/L)[104]. Subsequently, Gulyás et al.[183] performed [^{11}C]**18** imaging in healthy human subjects and reported rapid [^{11}C]**18** uptake in the brain. Radioactivity varied among different brain regions, with the greatest regional uptake in the thalamus, upper brain stem, striatum, and cortex, suggesting that [^{11}C]**18** binding was specific for TSPO. A PET imaging study in four MS patients demonstrated that global brain [^{11}C]**18** uptake significantly surpassed [^{11}C]**1** radioactivity, indicating that [^{11}C]**18** is superior to [^{11}C]**1**[184]. In contrast, Gulyás et al.[185] observed no significant differences in [^{11}C]**18** signal between AD patients and age-matched control subjects. In another study, Gulyás et al.[98] suggested that [^{11}C]**18** uptake in post-stroke patients was higher in the peri-infarct zone compared with the ischemic core; however, the difference was not significant. Additionally, no significant differences in BP were observed between [^{11}C]**18** and [^{11}C]**1** in any of the standard regions. This is likely due to the low binding affinity of [^{11}C]**18** for TSPO, which may limit further clinical use.

3.2.6. *Oxopurine analogs*

N-Benzyl-*N*-methyl-2-[7,8-dihydro-7-(2-^{18}F-fluoroethyl)-8-*oxo*-2-phenyl-9*H*-purin-9-yl] acetamide ([^{18}F]FEDAC [^{18}F]**19**, Fig. 2), is an ^{18}F-labeled oxopurine analog. The binding affinity (K_i) of [^{18}F]**19** toward TSPO was 1.34 ± 0.15 nmol/L *in vitro*, and [^{18}F]**19** had an appropriate lipophilicity (log$D$ = 3.1) [186]. [^{18}F]**19** showed high uptake (>1% ID/g) in the mouse brain, and [^{18}F]**19** radioactivity ranged from 1.33 ± 0.13 to 2.18 ± 0.33 in mouse bone, suggesting that little or no defluorination occurred. The maximum [^{18}F]**19** uptake in the monkey brain was in the occipital cortex at about 20 min p.i., similar to [^{11}C]**12**, and low accumulation of radioactivity was observed in the skull, suggesting little or no defluorination occurred *in vivo*. Metabolic analysis in brain homogenate demonstrated that 75% of [^{18}F]**19** was intact at 30 min p.i.[187]. Yanamoto et al.[188] found that [^{18}F]**19**

uptake in rat brain was substantially elevated in KA-lesioned striatum compared with non-lesioned striatum, indicating that [^{18}F]**19** is a potential PET tracer for TSPO imaging. Subsequently, Yui et al.[187] evaluated [^{18}F]**19** in the ischemic rat brain. They found that [^{18}F]**19** binding in the ischemic rat brain *in vivo* was significantly increased on the ipsilateral side compared with the contralateral side. Blocking studies with an excess of AC-5216 or PK11195 abolished the difference in radioactivity between the contralateral and ipsilateral sides. Similar results were also obtained by *ex vivo* autoradiography of infarcted rat brains[187]. Further investigation into the use of [^{18}F]**19** imaging to detect neuroinflammation in the primate and human brain is currently underway.

3.2.7. Acetamidobenzoxazolone

2-[5-(4-Methoxyphenyl)-2-oxo-1,3-benzoxazol-3(2*H*)-yl]-*N*-methyl-*N*-phenylacetamide (MBMP) is an acetamidobenzoxazolone skeleton labeled with ^{11}C and is a new candidate TSPO PET tracer ([^{11}C]**20**, Fig. 2). The binding affinity (K_i) of [^{11}C]**20** toward TSPO was 0.29 nmol/L, and [^{11}C]**20** had appropriate lipophilicity (clog$D$ = 3.5)[189]. [^{11}C]**20** rapidly entered the mouse brain. Initial brain uptake was more than 2.0% ID/g at 1 min p.i. in mice, and the maximum uptake was observed in the cerebellum. Metabolite analysis showed that 98.6 ± 0.5% of [^{11}C]**20** was intact at 5 min p.i. with one polar metabolite. However, at 60 min p.i., only 65.7 ± 2.7% of [^{11}C]**20** in the brain was intact. Subsequently, Tiwari et al.[189] evaluated TSPO binding radioligands in an ischemic rat model. Using PET imaging, they observed that [^{11}C]**20** and [^{11}C](*R*)**1** binding were obviously higher on the ipsilateral side than on the contralateral side. Blocking with unlabeled MBMP or PK11195 substantially decreased [^{11}C]**20** binding on the ipsilateral side. *In vitro* autoradiography yielded similar results. This suggested that [^{11}C]**20** was superior to [^{11}C](*R*)**1** for imaging. Critically, however, 35% of the [^{11}C]**20** signal observed in the mouse brain at 60 min p.i. came from radiometabolites, which is markedly higher than other TSPO radioligands (<10%)[79,138,168]. This is likely to limit the clinical use of ^{11}C-MBMP. Thus, further evaluation of [^{11}C]**20** was not warranted.

3.2.8. Aryloxypyridylamide

N-{2-[2-^{18}F-Fluoroethoxy]-5-methoxybenzyl}-*N*-[2-(4-methoxyphenoxy)pyridine-3-yl]acetamide [^{18}F]FEMPA [^{18}F]**21**, Fig. 2), is an aryloxypyridylamide derivative, and is a potential novel second-generation TSPO radioligand. Preclinical results suggested that [^{18}F]**21** could be rapidly eliminated from the brain and had a good SNR in nonhuman primates. Varrone et al.[190] demonstrated a markedly greater V_T for [^{18}F]**21** in the medial temporal cortex in AD patients compared with controls when the TSPO binding status was used as a covariate. They also observed a substantially higher V_T for [^{18}F]**21** in the medial and lateral temporal cortex, posterior cingulate, caudate, putamen, thalamus, and cerebellum in AD patients compared to controls. Their study suggested that [^{18}F]**21** could be used as a potential TSPO probe in AD patients if binding status is taken into account.

The second-generation TSPO radioligand properties and PET imaging studies are summarized in Supporting Information Table S2. Most of these PET tracers showed high affinity and high selectivity to TSPO and better SNR compared with [^{11}C]**1**. Thus, they have the potential to significantly contribute to clinical investigation of the relationship between TSPO and neurological disorders.

3.3. TSPO PET tracers with low binding sensitivity to rs6971 polymorphism

As mentioned above, a major limitation of aforementioned TSPO radioligands is TSPO binding affinity variability in the human brain[56,191,192]. This binding status variability is influenced by the single nucleotide polymorphism *rs6971* in the human *TSPO* gene, which has been classified as HAB (A/A; ~70%), MAB (A/T; ~21%), and LAB (T/T; ~9%)[193]. This polymorphism makes it difficult to generate consistent preclinical results with aforementioned TSPO radioligands. New radioligands that are insensitive to the *rs6971* polymorphism are needed (Fig. 3).

2-[5-(4-Fluoroethoxy-2-oxo-1,3-benzoxazol-3(2*H*)-yl)-*N*-methyl-*N*-phenylacetamide (FEBMP) is a novel TSPO ligand that can be labeled with ^{18}F for use as a radioligand ([^{18}F]**22**, Fig. 3)[194]. The binding affinity (K_i) of [^{18}F]**22** toward TSPO was 6.6 ± 0.7 nmol/L, and [^{18}F]**22** had a suitable lipophilicity (log$D$ = 3.43) *in vitro*[194]. A biodistribution study in mice demonstrated a relatively high initial [^{18}F]**22** radioactivity (approximately 2.7% ID/g) in the mouse brain at 1 min p.i. High uptake (approximately 3.8% ID/g) was also measured in mouse bone, which is not negligible. However, in the ischemic rat brain, there was very little [^{18}F]**22** accumulation in the skull. The investigators speculated that the uptake in mouse bone samples may have resulted from [^{18}F]**22** binding to marrow instead of [^{18}F]F^- trapped in bones. Metabolic analysis showed that parent [^{18}F]**22** remained at 76.4 ± 2.1% at 60 min p.i. in the mouse brain[195]. Subsequently, in a PET imaging study, Tiwari et al.[195] demonstrated that [^{18}F]**22** radioactivity in the ischemic rat brain was significantly increased in the ipsilateral striatum compared with the contralateral side. After pre-treatment with unlabeled MBMP or PK11195, the [^{18}F]**22** uptake was markedly decreased on the ipsilateral side of the brain, indicating that the [^{18}F]**22** signal was specific for TSPO.

Tiwari et al.[195] used [^{18}F]**22** to demonstrate the association of TSPO genotype with binding variability. *In vitro* autoradiographic analysis of postmortem human brains suggested that the [^{18}F]**22** K_i ratio for LAB to HAB ($R_{Ki(L/H)}$) was 0.9. The ratio of TSPO binding for LAB to HAB ($R_{B(L/H)}$) was also about 0.90. Thus, the ratio of specific binding for [^{18}F]**22** in both the HAB and LAB groups was similar, suggesting that the *rs6971* polymorphism didn't affect [^{18}F]**22** binding status. Further, their findings suggest that [^{18}F]**22** is a promising new tool for visualizing neuroinflammation[195]. However, *in vitro* results may differ from *in vivo* findings. Thus, further investigation of *in vivo* [^{18}F]**22** binding affinity in human subjects with different genotypes is needed.

(*S*-*N*,*N*-Diethyl-9-[2-^{18}F-fluoroethyl]-5-methoxy-2,3,4,9-tetrahydro-1*H*-carbazole-4-carboxamide) ([^{18}F]GE-180 [^{18}F]**23**, Fig. 3), is another promising TSPO radioligand used for human PET imaging[196]. [^{18}F]**23** has a very high affinity for TSPO (K_i = 2.4 nmol/L) in rat heart and metabolic analysis showed that 94% of [^{18}F]**23** was intact in the brain at 60 min p.i.[197], suggesting that [^{18}F]**23** is a very promising TSPO radioligand. In recent years, it has been widely used to study neuroinflammation. Wadsworth et al.[197] reported that [^{18}F]**23** had very good affinity, high brain absorption, and higher specific binding in a neuroinflammation model, and Dickens et al.[198] demonstrated that [^{18}F]**23** could identify sites of activated microglia in both gray and white matter in a LPS-induced model of acute neuroinflammation. They also suggested that [^{18}F]**23** could be

used to monitor activated microglia better than [^{11}C](*R*)**1** because of its higher BP and, as a fluorinated radioligand, its longer half-life. Similarly, Boutin et al.[199] reported that [^{18}F]**23** radioactivity in ischemic rat brains displayed a better SNR than [^{11}C]*R*-PK11195 due to its very low nonspecific binding. In another study, Liu et al.[200] showed that [^{18}F]**23** PET imaging could be used to monitor neuroinflammation during AD progression and treatment. Subsequently, López-Picón et al.[201] demonstrated that [^{18}F]23 could be used to monitor neuroinflammation and therapeutic modulation of microglial activation in an AD mouse model. Moreover [^{18}F]**23** imaging could also be used as a potential tool to study epileptogenesis in a rat model of TLE[202].

Feeney et al.[203] further demonstrated that the total V_T of [^{18}F]**23** were no significant correlations in either HAB and MAB. In one study of MS patients, Vomacka et al.[204] found that [^{18}F]**23** PET imaging could semi-quantitatively evaluate neuroinflammation in patients with relapsing remitting multiple sclerosis (RRMS). In a subsequent human study, Unterrainer et al.[205] demonstrated that [^{18}F]**23** PET imaging could detect areas of focal microglia activation in RRMS patient lesions that were not associated with the patient's binding genotype. They found that the SUVR of [^{18}F]**23** in the focal lesions of RRMS patients with different TSPO binding genotypes were 1.87 ± 0.43 (HAB), 1.95 ± 0.48 (MAB), and 1.86 ± 0.80 (LAB). However, another recent study showed that [^{18}F]**23** had very low brain uptake in human subjects, hindering its translation to human PET imaging[206].

Another new TSPO radioligand [^{11}C](*R*)-*N*-sec-butyl-4-(2-chlorophenyl)-*N*-methylquinazoline-2-carboxamide ([^{11}C]ER176 [^{11}C]**24**, Fig. 3), is a novel quinazoline analog of [^{11}C](*R*)**1** [^{11}C]**24** has adequately high binding affinity for all TSPO *rs6971* genotypes[207]. The ratio of radioligand binding in HAB to LAB was only 1.3 to 1 for ER176 in human brain tissue[208], whereas the comparable ratio was 55 to 1 for PBR28[56]. Nevertheless, the clinical relevance of this compound remains to be confirmed.

The latest TSPO radioligand [^{18}F]GE387 ([^{18}F]**25**, Fig. 3), was recently reported by Qiao et al.[209]. More importantly, the binding affinities of [^{18}F](*S*)**25** to LAB and HAB were evaluated using an assay based on human embryonic kidney cell lines, and the LAB/HAB ratio was determined to be 1.3, which was similar to that of [^{11}C](*R*)**1**. This suggests that [^{18}F]**25** TSPO binding affinity is not influenced by TSPO genotype. Moreover, they also showed that the racemic analogue of [^{18}F]**25** could enter the brain in wild-type rats. Thus [^{18}F]**25** has high potential as a TSPO radioligand due to its long half-life and probably low sensitivity to the human *rs6971* polymorphism[209]. However, further [^{18}F]**25** PET imaging studies need to be performed in non-human primates and humans. These new TSPO radioligands properties and PET imaging studies are summarized in Supporting Information Table S3. Although these TSPO radioligands are less sensitive TSPO binding variability compared with aforementioned radioligands, their detection was still inconsistent, limiting further comparisons. Further clinical studies are needed to evaluate these new third-generation TSPO radioligands.

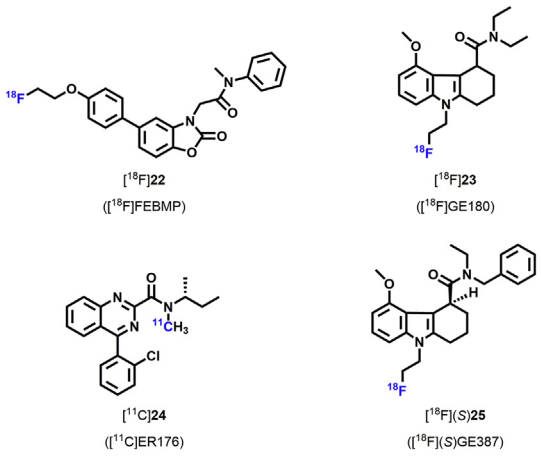

Figure 3 Chemical structures of new TSPO radioligands with insensitivity to *rs6971*.

4. Conclusions and perspectives

A candidate PET radioligand must meet a wide array of chemical and biochemical requirements[210], including (i) high binding affinity represented by K_i or half-maximal inhibitory concentration (IC_{50})—the ligands should generally have high affinity for imaging brain targets in the nanomolar or subnanomolar range; (ii) selectivity for target binding—the ligand should bind only to the biomarker, and possesses weak affinity for off-target sites; (iii) ability to pass the BBB [generally molecular weight MW < 400 Da, appropriate lipophilicity ($\log D_{7.4}$ of 1−3)]; (iv) amenability to be labeled with carbon-11 or fluorine-18. When the ligand is optimized and radiolabeled, the corresponding radioactive PET tracer should (v) have relatively high radiochemical yields (ideally >10%); (vi) show high *BP*, low nonspecific binding (or low nondisplaceable binding) and rapid clearance for nonspecific binding; (vii) be lack of accumulation of radiometabolites in the brain or radiodefluorination in skull. Specificity for TSPO, receptor binding assays at the cellular level derived from human[192,209] would facilitate the discovery of novel ligands with low sensitive or insensitive to genotype, which would be helpful to develop next-generation TSPO PET tracers since traditional PET imaging in rodents or monkeys could not distinguish this *rs6971* polymorphism.

However, the rational design of TSPO PET radiotracers with low sensitivity to the A147T variant encounter challenges. So far, only one crystal structure of TSPO with PK11195 was disclosed (Fig. 1), and A147T TSPO was capable of retaining the uniform structural and dynamic profile of TSPO and thus binds PK11195 with similar affinity[211], making this ligand as a promising scaffold for further *rs6971*-polymorphism-insensitive tracer development[10,212]. Scarf et al.[85] proposed that this is due to a poor understanding of how ligands bind with TSPO and a lack of knowledge about how the protein changes in disease states. Thus, a more comprehensive understanding of binding mode of the ligand to TSPO, and biological structure changes of TSPO in disease states are necessary to enable the development of more specific PET radiotracers that provide significant insights into the role of TSPO in neuroinflammation.

Although great efforts have been made over the past decades to develop new TSPO radioligands for visualizing neuroinflammation in clinical research, there are a number of nuances that influence the interpretation of TSPO. These issues are not specific to TSPO, and are typical of neuroinflammatory markers in brain, however, they do illustrate that it would be useful to have additional markers of gliosis for *in vivo* imaging.

While it is well described that TSPO is overexpressed in a number of diseases with microglial and astroglial activation, TSPO is located on the mitochondria. Hence, it is theoretically

possible that mitochondrial loss could result in a reduction in signal in some diseases and obscure a positive finding if the magnitude of signal loss due to lower mitochondrial density matched the greater expression of TSPO from gliosis. Also, it is possible that as more is learned about TSPO, other factors will be determined that might affect its expression since TSPO has a number of roles as discussed in the introduction. In addition, TSPO expression is not fully selective to activated microglia. Inflammatory cells of different types may adopt similar mechanisms and protein expression for common cellular functions. In disease states, TSPO may be found in activated microglia, astrocytes, and sometimes peripheral macrophages[27,28,76,77]. In health, TSPO may be found in endothelial cells and undifferentiated $GFAP^+$ neural stem cells[213]. Hence the differential elevation in TSPO binding between health and disease is typically viewed as reflecting microglial and astroglial activation[213].

To address these issues other radiotracers are being developed for novel targets[214–216]. New radiotracers for the membrane purinergic receptor $P2X_7$ ($P2X_7R$) are under development[217]. Recent studies have compared PET imaging using [^{18}F]**15** (a second-generation TSPO radioligand) and [^{11}C]JNJ717 (a novel PET tracer for $P2X_7R$) in patients with ALS[218]. The results indicated that [^{18}F]**15** uptake in motor cortex was visually enhanced and could co-localize with Iba1 staining, but not GFAP staining, in ALS. However, they didn't monitor the regional increase in [^{11}C]JNJ717 binding or the co-localization of [^{11}C]JNJ717 and Iba1/GFAP staining. These findings suggest that TSPO imaging may be superior to $P2X_7R$ imaging in early symptomatic ALS patients[218]. Other cautions of the $P2X_7$ radiotracers is that they also bind to astrocytes, and the variability of their binding in healthy humans is high[219]. However, it has been proposed that identification of genotypes associated with this variance might be applied as a similar strategy as with TSPO radioligands[219]. Monoamine oxidase B (MAO-B) is overexpressed in activated astroglia in neurodegenerative diseases such as AD and several MAO-B radioligands have been modeled in humans, of which SL25.1188 has been shown to have the best properties of reversibility, brain uptake, and lack of brain penetrant metabolites[220]. To date SL2511.88 has been applied in MDD for which greater MAO-B V_T was identified in the prefrontal cortex, and greater MAO-B V_T was found with age, the latter which was attributed to greater astrogliosis with disease progression in MDD[221]. Thus, radioligands development for studying neuroinflammation remains to be further explored.

5. Future directions

TSPO is widely distributed throughout the whole body and is especially enriched in tissues that synthesize steroids. TSPO is mainly located in the OMM, linking signaling between the OMM and the IMM at the subcellular level. A dramatic upregulation of TSPO is associated with microglial activation in response to brain injury and neuroinflammation. Therefore, elevated TSPO expression is considered a hallmark of gliosis and microglial activation. TSPO radioligands may be utilized to assess gliosis in neuropsychiatric diseases and, in the future, their treatment. Currently, many TSPO PET tracers have been developed and widely used, however, because of the *rs6971 TSPO* polymorphism, there is not yet a suitable TSPO PET tracer for patients with a genetically determined low binding affinity. In addition, it would be ideal if more specific radioligands as well as biomarkers for activated microglia were developed. Additional studies are needed to conduct preclinical and early clinical assessment of these PET tracers, especially those radiolabeled with ^{18}F, in order to establish their usefulness as research and clinical tools. There is great potential for the future use of these radioligands as diagnostic and prognostic tools, as well as for assessing therapeutic interventions for neurologic diseases.

Acknowledgments

We thank Dr. Jeffrey H. Meyer, Neil Vasdev, and Steven H. Liang for modifying the paper. The authors gratefully acknowledge the support of K.C. Wong Education Foundation (China), and the Project of Innovative Team for the Guangdong Universities (2018KCXTD001, China). This work was financially supported by the National Natural Science Foundation of China (Nos. 81701751 and 81871383) and Guangdong Basic and Applied Basic Research Foundation (2020A1515011192, China).

Author contributions

Lingling Zhang and Kuan Hu contributed to the writing of the manuscript. Lu Hou and Shaojuan Zhang constructed the Figures and Tables. Jinghao Wang and Hao Xu provided constructive suggestions. Tuo Shao and Weijian Ye contributed to the English language editing. Lee Josephson, Jeffrey H. Meyer, Ming-Rong Zhang and Neil Vasdev modified the paper. Lu Wang and Steven H. Liang conceived the project and modified the paper.

Conflicts of interest

The authors declare no conflicts of interest.

Appendix A. Supporting information

Supporting data to this article can be found online at https://doi.org/10.1016/j.apsb.2020.08.006.

References

1. Papadopoulos V, Baraldi M, Guilarte TR, Knudsen TB, Lacapère JJ, Lindemann P, et al. Translocator protein (18kDa): new nomenclature for the peripheral-type benzodiazepine receptor based on its structure and molecular function. *Trends Pharmacol Sci* 2006;**27**:402–9.
2. Guilarte TR. TSPO in diverse CNS pathologies and psychiatric disease: a critical review and a way forward. *Pharmacol Ther* 2019;**194**:44–58.
3. Liu GJ, Middleton RJ, Hatty CR, Kam WW, Chan R, Pham T, et al. The 18 kDa translocator protein, microglia and neuroinflammation. *Brain Pathol* 2014;**24**:631–53.
4. Li H, Papadopoulos V. Peripheral-type benzodiazepine receptor function in cholesterol transport. Identification of a putative cholesterol recognition/interaction amino acid sequence and consensus pattern. *Endocrinology* 1998;**139**:4991–7.
5. Jamin N, Neumann JM, Ostuni MA, Vu TK, Yao ZX, Murail S, et al. Characterization of the cholesterol recognition amino acid consensus sequence of the peripheral-type benzodiazepine receptor. *Mol Endocrinol* 2005;**19**:588–94.
6. Lacapère JJ, Delavoie F, Li H, Péranzi G, Maccario J, Papadopoulos V, et al. Structural and functional study of reconstituted peripheral benzodiazepine receptor. *Biochem Biophys Res Commun* 2001;**284**:536–41.

7. Gatliff J, Campanella M. TSPO: kaleidoscopic 18-kDa amid biochemical pharmacology, control and targeting of mitochondria. *Biochem J* 2016;**473**:107−21.
8. Gatliff J, East D, Crosby J, Abeti R, Harvey R, Craigen W, et al. TSPO interacts with VDAC1 and triggers a ROS-mediated inhibition of mitochondrial quality control. *Autophagy* 2014;**10**:2279−96.
9. Guo Y, Kalathur RC, Liu Q, Kloss B, Bruni R, Ginter C, et al. Protein structure. Structure and activity of tryptophan-rich TSPO proteins. *Science* 2015;**347**:551−5.
10. Li F, Liu J, Zheng Y, Garavito RM, Ferguson-Miller S. Protein structure. Crystal structures of translocator protein (TSPO) and mutant mimic of a human polymorphism. *Science* 2015;**347**:555−8.
11. Santoro A, Mattace Raso G, Taliani S, Da Pozzo E, Simorini F, Costa B, et al. TSPO-ligands prevent oxidative damage and inflammatory response in C6 glioma cells by neurosteroid synthesis. *Eur J Pharmaceut Sci* 2016;**88**:124−31.
12. Veenman L, Gavish M. The peripheral-type benzodiazepine receptor and the cardiovascular system. Implications for drug development. *Pharmacol Ther* 2006;**110**:503−24.
13. Larcher JC, Vayssiere JL, Le Marquer FJ, Cordeau LR, Keane PE, Bachy A, et al. Effects of peripheral benzodiazepines upon the O_2 consumption of neuroblastoma cells. *Eur J Pharmacol* 1989;**161**: 197−202.
14. Ritsner M, Modai I, Gibel A, Leschiner S, Silver H, Tsinovoy G, et al. Decreased platelet peripheral-type benzodiazepine receptors in persistently violent schizophrenia patients. *J Psychiatr Res* 2003;**37**: 549−56.
15. O'Hara MF, Nibbio BJ, Craig RC, Nemeth KR, Charlap JH, Knudsen TB. Mitochondrial benzodiazepine receptors regulate oxygen homeostasis in the early mouse embryo. *Reprod Toxicol* 2003;**17**: 365−75.
16. Galiègue S, Casellas P, Kramar A, Tinel N, Simony-Lafontaine J. Immunohistochemical assessment of the peripheral benzodiazepine receptor in breast cancer and its relationship with survival. *Clin Canc Res* 2004;**10**:2058−64.
17. Hauet T, Yao ZX, Bose HS, Wall CT, Han Z, Li W, et al. Peripheral-type benzodiazepine receptor-mediated action of steroidogenic acute regulatory protein on cholesterol entry into leydig cell mitochondria. *Mol Endocrinol* 2005;**19**:540−54.
18. O'Hara MF, Charlap JH, Craig RC, Knudsen TB. Mitochondrial transduction of ocular teratogenesis during methylmercury exposure. *Teratology* 2002;**65**:131−44.
19. Ostuni MA, Marazova K, Peranzi G, Vidic B, Papadopoulos V, Ducroc R, et al. Functional characterization and expression of PBR in rat gastric mucosa: stimulation of chloride secretion by PBR ligands. *Am J Physiol Gastrointest Liver Physiol* 2004;**286**: G1069−80.
20. Pulagam KR, Colás L, Padro D, Plaza-García S, Gómez-Vallejo V, Higuchi M, et al. Evaluation of the novel TSPO radiotracer [^{18}F] VUIIS1008 in a preclinical model of cerebral ischemia in rats. *EJNMMI Res* 2017;**7**:93.
21. Papadopoulos V, Lecanu L, Brown RC, Han Z, Yao ZX. Peripheral-type benzodiazepine receptor in neurosteroid biosynthesis, neuropathology and neurological disorders. *Neuroscience* 2006;**138**:749−56.
22. Veenman L, Leschiner S, Spanier I, Weisinger G, Weizman A, Gavish M. PK11195 attenuates kainic acid-induced seizures and alterations in peripheral-type benzodiazepine receptor (PBR) protein components in the rat brain. *J Neurochem* 2002;**80**:917−27.
23. Leonelli E, Yague JG, Ballabio M, Azcoitia I, Magnaghi V, Schumacher M, et al. Ro5-4864, a synthetic ligand of peripheral benzodiazepine receptor, reduces aging-associated myelin degeneration in the sciatic nerve of male rats. *Mech Ageing Dev* 2005;**126**: 1159−63.
24. Knezevic D, Mizrahi R. Molecular imaging of neuroinflammation in Alzheimer's disease and mild cognitive impairment. *Prog Neuro-Psychopharmacol Biol Psychiatry* 2018;**80**:123−31.
25. Lavisse S, Guillermier M, Hérard AS, Petit F, Delahaye M, Van Camp N, et al. Reactive astrocytes overexpress TSPO and are detected by TSPO positron emission tomography imaging. *J Neurosci* 2012;**32**:10809−18.
26. Dupont AC, Largeau B, Santiago Ribeiro MJ, Guilloteau D, Tronel C, Arlicot N. Translocator protein-18 kDa (TSPO) positron emission tomography (PET) imaging and its clinical impact in neurodegenerative diseases. *Int J Mol Sci* 2017;**18**:785.
27. Cosenza-Nashat M, Zhao ML, Suh HS, Morgan J, Natividad R, Morgello S, et al. Expression of the translocator protein of 18 kDa by microglia, macrophages and astrocytes based on immunohistochemical localization in abnormal human brain. *Neuropathol Appl Neurobiol* 2009;**35**:306−28.
28. Venneti S, Wang G, Nguyen J, Wiley CA. The positron emission tomography ligand DAA1106 binds with high affinity to activated microglia in human neurological disorders. *J Neuropathol Exp Neurol* 2008;**67**:1001−10.
29. Gershen LD, Zanotti-Fregonara P, Dustin IH, Liow JS, Hirvonen J, Kreisl WC, et al. Neuroinflammation in temporal lobe epilepsy measured using positron emission tomographic imaging of translocator protein. *JAMA Neurol* 2015;**72**:882−8.
30. Setiawan E, Wilson AA, Mizrahi R, Rusjan PM, Miler L, Rajkowska G, et al. Role of translocator protein density, a marker of neuroinflammation, in the brain during major depressive episodes. *JAMA Psychiatry* 2015;**72**:268−75.
31. Phelps ME. Positron emission tomography provides molecular imaging of biological processes. *Proc Natl Acad Sci U S A* 2000;**97**: 9226−33.
32. Willmann JK, van Bruggen N, Dinkelborg LM, Gambhir SS. Molecular imaging in drug development. *Nat Rev Drug Discov* 2008;**7**: 591−607.
33. Ametamey SM, Honer M, Schubiger PA. Molecular imaging with PET. *Chem Rev* 2008;**108**:1501−16.
34. Huang H, Zhu H, Xie Q, Tian X, Yang X, Feng F, et al. Evaluation of ^{124}I-JS001 for hPD1 immuno-PET imaging using sarcoma cell homografts in humanized mice. *Acta Pharm Sin B* 2020;**10**:1321−30.
35. Suridjan I, Comley RA, Rabiner EA. The application of positron emission tomography (PET) imaging in CNS drug development. *Brain Imaging Behav* 2019;**13**:354−65.
36. Deng X, Rong J, Wang L, Vasdev N, Zhang L, Josephson L, et al. Chemistry for positron emission tomography: recent advances in ^{11}C-, ^{18}F-, ^{13}N-, and ^{15}O-labeling reactions. *Angew Chem Int Ed Engl* 2019;**58**:2580−605.
37. Lan Y, Bai P, Chen Z, Neelamegam R, Placzek MS, Wang H, et al. Novel radioligands for imaging sigma-1 receptor in brain using positron emission tomography (PET). *Acta Pharm Sin B* 2019;**9**: 1204−15.
38. Park SY, Zacharias C, Harrison C, Fan RE, Kunder C, Hatami N, et al. Gallium 68 PSMA-11 PET/MR imaging in patients with intermediate- or high-risk prostate cancer. *Radiology* 2018;**288**: 495−505.
39. Hu K, Shang J, Xie L, Hanyu M, Zhang Y, Yang Z, et al. PET Imaging of VEGFR with a novel ^{64}Cu-labeled peptide. *ACS Omega* 2020;**5**:8508−14.
40. Bensch F, van der Veen EL, Lub-de Hooge MN, Jorritsma-Smit A, Boellaard R, Kok IC, et al. ^{89}Zr-atezolizumab imaging as a non-invasive approach to assess clinical response to PD-L1 blockade in cancer. *Nat Med* 2018;**24**:1852−8.
41. Li D, Cheng S, Zou S, Zhu D, Zhu T, Wang P, et al. Immuno-PET imaging of ^{89}Zr labeled anti-PD-L1 domain antibody. *Mol Pharm* 2018;**15**:1674−81.
42. Hu K, Xie L, Zhang Y, Hanyu M, Yang Z, Nagatsu K, et al. Marriage of black phosphorus and Cu^{2+} as effective photothermal agents for PET-guided combination cancer therapy. *Nat Commun* 2020;**11**: 2778.
43. Hou L, Wang L, Wang J, Ye W, Wu X, Zheng Z, et al. Positron emission tomography (PET) application in the phase 0 clinical trials in drug development. *Pharm Today* 2020;**30**:99−105.
44. Coughlin JM, Wang Y, Minn I, Bienko N, Ambinder EB, Xu X, et al. Imaging of glial cell activation and white matter integrity in brains of

active and recently retired national football league players. *JAMA Neurol* 2017;**74**:67−74.
45. Sucksdorff M, Rissanen E, Tuisku J, Nuutinen S, Paavilainen T, Rokka J, et al. Evaluation of the effect of fingolimod treatment on microglial activation using serial PET imaging in multiple sclerosis. *J Nucl Med* 2017;**58**:1646−51.
46. Morris RS, Simon Jones P, Alawneh JA, Hong YT, Fryer TD, Aigbirhio FI, et al. Relationships between selective neuronal loss and microglial activation after ischaemic stroke in man. *Brain* 2018;**141**: 2098−111.
47. Yokokura M, Terada T, Bunai T, Nakaizumi K, Takebayashi K, Iwata Y, et al. Depiction of microglial activation in aging and dementia: positron emission tomography with [^{11}C]DPA713 *versus* [^{11}C](*R*)PK11195. *J Cerebr Blood Flow Metabol* 2017;**37**:877−89.
48. Politis M, Lahiri N, Niccolini F, Su P, Wu K, Giannetti P, et al. Increased central microglial activation associated with peripheral cytokine levels in premanifest Huntington's disease gene carriers. *Neurobiol Dis* 2015;**83**:115−21.
49. Datta G, Colasanti A, Rabiner EA, Gunn RN, Malik O, Ciccarelli O, et al. Neuroinflammation and its relationship to changes in brain volume and white matter lesions in multiple sclerosis. *Brain* 2017; **140**:2927−38.
50. Kobayashi M, Jiang T, Telu S, Zoghbi SS, Gunn RN, Rabiner EA, et al. ^{11}C-DPA-713 has much greater specific binding to translocator protein 18 kDa (TSPO) in human brain than ^{11}C-(*R*)-PK11195. *J Cerebr Blood Flow Metabol* 2018;**38**:393−403.
51. Datta G, Colasanti A, Kalk N, Owen D, Scott G, Rabiner EA, et al. ^{11}C-PBR28 and ^{18}F-PBR111 detect white matter inflammatory heterogeneity in multiple sclerosis. *J Nucl Med* 2017;**58**:1477−82.
52. Brody AL, Hubert R, Enoki R, Garcia LY, Mamoun MS, Okita K, et al. Effect of cigarette smoking on a marker for neuroinflammation: a [^{11}C]DAA1106 positron emission tomography study. *Neuropsychopharmacology* 2018;**43**:925.
53. Vignal N, Cisternino S, Rizzo-Padoin N, San C, Hontonnou F, Gelé T, et al. [^{18}F]FEPPA a TSPO radioligand: optimized radiosynthesis and evaluation as a PET radiotracer for brain inflammation in a peripheral LPS-injected mouse model. *Molecules* 2018;**23**:1375.
54. Fan Z, Harold D, Pasqualetti G, Williams J, Brooks DJ, Edison P. Can studies of neuroinflammation in a TSPO genetic subgroup (HAB or MAB) be applied to the entire AD cohort?. *J Nucl Med* 2015;**56**: 707−13.
55. Lin D, Chang YJ, Strauss 3rd JF, Miller WL. The human peripheral benzodiazepine receptor gene: cloning and characterization of alternative splicing in normal tissues and in a patient with congenital lipoid adrenal hyperplasia. *Genomics* 1993;**18**:643−50.
56. Kreisl WC, Jenko KJ, Hines CS, Lyoo CH, Corona W, Morse CL, et al. A genetic polymorphism for translocator protein 18 kDa affects both *in vitro* and *in vivo* radioligand binding in human brain to this putative biomarker of neuroinflammation. *J Cerebr Blood Flow Metabol* 2013;**33**:53−8.
57. Sandiego CM, Gallezot JD, Pittman B, Nabulsi N, Lim K, Lin SF, et al. Imaging robust microglial activation after lipopolysaccharide administration in humans with PET. *Proc Natl Acad Sci U S A* 2015; **112**:12468−73.
58. Heneka MT, Carson MJ, El Khoury J, Landreth GE, Brosseron F, Feinstein DL, et al. Neuroinflammation in Alzheimer's disease. *Lancet Neurol* 2015;**14**:388−405.
59. Kreisl WC, Lyoo CH, McGwier M, Snow J, Jenko KJ, Kimura N, et al. *In vivo* radioligand binding to translocator protein correlates with severity of Alzheimer's disease. *Brain* 2013;**136**:2228−38.
60. Liu B, Hong JS. Role of microglia in inflammation-mediated neurodegenerative diseases: mechanisms and strategies for therapeutic intervention. *J Pharmacol Exp Therapeut* 2003;**304**:1−7.
61. McGeer EG, McGeer PL. Neuroinflammation in Alzheimer's disease and mild cognitive impairment: a field in its infancy. *J Alzheimers Dis* 2010;**19**:355−61.
62. Heppner FL, Ransohoff RM, Becher B. Immune attack: the role of inflammation in Alzheimer disease. *Nat Rev Neurosci* 2015;**16**: 358−72.
63. Schwab C, McGeer PL. Inflammatory aspects of Alzheimer disease and other neurodegenerative disorders. *J Alzheimers Dis* 2008;**13**: 359−69.
64. Streit WJ. Microglia as neuroprotective, immunocompetent cells of the CNS. *Glia* 2002;**40**:133−9.
65. Peferoen LA, Vogel DY, Ummenthum K, Breur M, Heijnen PD, Gerritsen WH, et al. Activation status of human microglia is dependent on lesion formation stage and remyelination in multiple sclerosis. *J Neuropathol Exp Neurol* 2015;**74**:48−63.
66. Rupprecht R, Papadopoulos V, Rammes G, Baghai TC, Fan J, Akula N, et al. Translocator protein (18 kDa) (TSPO) as a therapeutic target for neurological and psychiatric disorders. *Nat Rev Drug Discov* 2010;**9**:971−88.
67. Scarf AM, Ittner LM, Kassiou M. The translocator protein (18 kDa): central nervous system disease and drug design. *J Med Chem* 2009; **52**:581−92.
68. Chen MK, Guilarte TR. Translocator protein 18 kDa (TSPO): molecular sensor of brain injury and repair. *Pharmacol Ther* 2008;**118**: 1−17.
69. Venneti S, Lopresti BJ, Wang G, Bissel SJ, Mathis CA, Meltzer CC, et al. PET imaging of brain macrophages using the peripheral benzodiazepine receptor in a macaque model of neuroAIDS. *J Clin Invest* 2004;**113**:981−9.
70. McGeer PL, Itagaki S, Boyes BE, McGeer EG. Reactive microglia are positive for HLA-DR in the substantia nigra of Parkinson's and Alzheimer's disease brains. *Neurology* 1988;**38**:1285−91.
71. Tiwari PC, Pal R. The potential role of neuroinflammation and transcription factors in Parkinson disease. *Dialogues Clin Neurosci* 2017;**19**:71−80.
72. Haukedal H, Freude K. Implications of microglia in amyotrophic lateral sclerosis and frontotemporal dementia. *J Mol Biol* 2019;**431**: 1818−29.
73. McCauley ME, Baloh RH. Inflammation in ALS/FTD pathogenesis. *Acta Neuropathol* 2019;**137**:715−30.
74. Wimmer I, Scharler C, Zrzavy T, Kadowaki T, Mödlagl V, Rojc K, et al. Microglia pre-activation and neurodegeneration precipitate neuroinflammation without exacerbating tissue injury in experimental autoimmune encephalomyelitis. *Acta Neuropathol Commun* 2019;**7**:14.
75. Attwells S, Setiawan E, Wilson AA, Rusjan PM, Mizrahi R, Miler L, et al. Inflammation in the neurocircuitry of obsessive-compulsive disorder. *JAMA Psychiatry* 2017;**74**:833−40.
76. Martín A, Boisgard R, Thézé B, Van Camp N, Kuhnast B, Damont A, et al. Evaluation of the PBR/TSPO radioligand [^{18}F]DPA-714 in a rat model of focal cerebral ischemia. *J Cerebr Blood Flow Metabol* 2010;**30**:230−41.
77. Banati RB, Myers R, Kreutzberg GW. PK ('peripheral benzodiazepine')–binding sites in the CNS indicate early and discrete brain lesions: microautoradiographic detection of [^{3}H]PK11195 binding to activated microglia. *J Neurocytol* 1997;**26**:77−82.
78. Tang D, Fujinaga M, Hatori A, Zhang Y, Yamasaki T, Xie L, et al. Evaluation of the novel TSPO radiotracer 2-(7-butyl-2-(4-(2-([^{18}F] fluoroethoxy)phenyl)-5-methylpyrazolo[1,5-*a*]pyrimidin-3-yl)-*N,N*-diethylacetamide in a preclinical model of neuroinflammation. *Eur J Med Chem* 2018;**150**:1−8.
79. Wilson AA, Garcia A, Parkes J, McCormick P, Stephenson KA, Houle S, et al. Radiosynthesis and initial evaluation of [^{18}F]-FEPPA for PET imaging of peripheral benzodiazepine receptors. *Nucl Med Biol* 2008;**35**:305−14.
80. Zhang MR, Kumata K, Maeda J, Yanamoto K, Hatori A, Okada M, et al. ^{11}C-AC-5216: a novel PET ligand for peripheral benzodiazepine receptors in the primate brain. *J Nucl Med* 2007;**48**: 1853−61.

81. Rotstein BH, Wang L, Liu RY, Patteson J, Kwan EE, Vasdev N, et al. Mechanistic studies and radiofluorination of structurally diverse pharmaceuticals with spirocyclic Iodonium (III) ylides. *Chem Sci* 2016;**7**:4407−17.
82. Camsonne R, Crouzel C, Comar D, Mazière M, Prenant C, Sastre J, et al. Synthesis of *N*-(^{11}C) methyl, *N*-(methyl-1 propyl), (chloro-2 phenyl)-1 isoquinoleine carboxamide-3 (PK11195): a new ligand for peripheral benzodiazepine receptors. *J Label Compd Radiopharm* 1984;**21**:985−91.
83. Cagnin A, Gerhard A, Banati RB. *In vivo* imaging of neuroinflammation. *Eur Neuropsychopharmacol* 2002;**12**:581−6.
84. Shah F, Hume SP, Pike VW, Ashworth S, McDermott J. Synthesis of the enantiomers of [*N*-methyl-^{11}C]PK11195 and comparison of their behaviours as radioligands for PK binding sites in rats. *Nucl Med Biol* 1994;**21**:573−81.
85. Scarf AM, Kassiou M. The translocator protein. *J Nucl Med* 2011;**52**:677−80.
86. Kropholler MA, Boellaard R, Schuitemaker A, Folkersma H, van Berckel BN, Lammertsma AA. Evaluation of reference tissue models for the analysis of [^{11}C](*R*)-PK11195 studies. *J Cerebr Blood Flow Metabol* 2006;**26**:1431−41.
87. Parbo P, Ismail R, Hansen KV, Amidi A, Mårup FH, Gottrup H, et al. Brain inflammation accompanies amyloid in the majority of mild cognitive impairment cases due to Alzheimer's disease. *Brain* 2017;**140**:2002−11.
88. Fan Z, Aman Y, Ahmed I, Chetelat G, Landeau B, Ray Chaudhuri K, et al. Influence of microglial activation on neuronal function in Alzheimer's and Parkinson's disease dementia. *Alzheimers Dement* 2015;**11**:608−621.e7.
89. Kübler D, Wächter T, Cabanel N, Su Z, Turkheimer FE, Dodel R, et al. Widespread microglial activation in multiple system atrophy. *Mov Disord* 2019;**34**:564−8.
90. Passamonti L, Rodríguez PV, Hong YT, Allinson KSJ, Bevan-Jones WR, Williamson D, et al. [^{11}C]PK11195 binding in Alzheimer disease and progressive supranuclear palsy. *Neurology* 2018;**90**:e1989−96.
91. Gerhard A, Watts J, Trender-Gerhard I, Turkheimer F, Banati RB, Bhatia K, et al. *In vivo* imaging of microglial activation with [^{11}C](*R*)-PK11195 PET in corticobasal degeneration. *Mov Disord* 2004;**19**:1221−6.
92. Cagnin A, Rossor M, Sampson EL, Mackinnon T, Banati RB. *In vivo* detection of microglial activation in frontotemporal dementia. *Ann Neurol* 2004;**56**:894−7.
93. Iannaccone S, Cerami C, Alessio M, Garibotto V, Panzacchi A, Olivieri S, et al. *In vivo* microglia activation in very early dementia with Lewy bodies, comparison with Parkinson's disease. *Park Relat Disord* 2013;**19**:47−52.
94. Ghadery C, Koshimori Y, Coakeley S, Harris M, Rusjan P, Kim J, et al. Microglial activation in Parkinson's disease using [^{18}F]-FEPPA. *J Neuroinflammation* 2017;**14**:8.
95. Plavén-Sigray P, Schain M, Zanderigo F, Rabiner EA, Gunn RN, Ogden RT, et al. Accuracy and reliability of [^{11}C]PBR28 specific binding estimated without the use of a reference region. *Neuroimage* 2019;**188**:102−10.
96. Brody AL, Gehlbach D, Garcia LY, Enoki R, Hoh C, Vera D, et al. Effect of overnight smoking abstinence on a marker for microglial activation: a [^{11}C]DAA1106 positron emission tomography study. *Psychopharmacology (Berl)* 2018;**235**:3525−34.
97. Terada T, Yokokura M, Yoshikawa E, Futatsubashi M, Kono S, Konishi T, et al. Extrastriatal spreading of microglial activation in Parkinson's disease: a positron emission tomography study. *Ann Nucl Med* 2016;**30**:579−87.
98. Gulyás B, Toth M, Vas A, Shchukin E, Kostulas K, Hillert J, et al. Visualising neuroinflammation in post-stroke patients: a comparative PET study with the TSPO molecular imaging biomarkers [^{11}C]PK11195 and [^{11}C]vinpocetine. *Curr Rad* 2012;**5**:19−28.
99. Yui J, Hatori A, Kawamura K, Yanamoto K, Yamasaki T, Ogawa M, et al. Visualization of early infarction in rat brain after ischemia using a translocator protein (18 kDa) PET ligand [^{11}C]DAC with ultra-high specific activity. *Neuroimage* 2011;**54**:123−30.
100. Singhal T, O'Connor K, Dubey S, Belanger AP, Hurwitz S, Chu R, et al. ^{18}F-PBR06 *versus* ^{11}C-PBR28 PET for assessing white matter translocator protein binding in multiple sclerosis. *Clin Nucl Med* 2018;**43**:e289−95.
101. Hamelin L, Lagarde J, Dorothée G, Potier MC, Corlier F, Kuhnast B, et al. Distinct dynamic profiles of microglial activation are associated with progression of Alzheimer's disease. *Brain* 2018;**141**:1855−70.
102. Colasanti A, Guo Q, Giannetti P, Wall MB, Newbould RD, Bishop C, et al. Hippocampal neuroinflammation, functional connectivity, and depressive symptoms in multiple sclerosis. *Biol Psychiatr* 2016;**80**:62−72.
103. Vivash L, O'Brien TJ. Imaging microglial activation with TSPO PET: lighting up neurologic diseases?. *J Nucl Med* 2016;**57**:165−8.
104. Alam MM, Lee J, Lee SY. Recent progress in the development of TSPO PET ligands for neuroinflammation imaging in neurological diseases. *Nucl Med Mol Imaging* 2017;**51**:283−96.
105. Wang M, Gao M, Zheng QH. Fully automated synthesis of PET TSPO radioligands [^{11}C]DAA1106 and [^{18}F]FEDAA1106. *Appl Radiat Isot* 2012;**70**:965−73.
106. Venneti S, Lopresti BJ, Wang G, Slagel SL, Mason NS, Mathis CA, et al. A comparison of the high-affinity peripheral benzodiazepine receptor ligands DAA1106 and (*R*)-PK11195 in rat models of neuroinflammation: implications for PET imaging of microglial activation. *J Neurochem* 2007;**102**:2118−31.
107. Chaki S, Funakoshi T, Yoshikawa R, Okuyama S, Okubo T, Nakazato A, et al. Binding characteristics of [^{3}H]DAA1106, a novel and selective ligand for peripheral benzodiazepine receptors. *Eur J Pharmacol* 1999;**371**:197−204.
108. Maeda J, Suhara T, Zhang MR, Okauchi T, Yasuno F, Ikoma Y, et al. Novel peripheral benzodiazepine receptor ligand [^{11}C]DAA1106 for PET: an imaging tool for glial cells in the brain. *Synapse* 2004;**52**:283−91.
109. Zhang MR, Kida T, Noguchi J, Furutsuka K, Maeda J, Suhara T, et al. [^{11}C]DAA1106: radiosynthesis and *in vivo* binding to peripheral benzodiazepine receptors in mouse brain. *Nucl Med Biol* 2003;**30**:513−9.
110. Venneti S, Wagner AK, Wang G, Slagel SL, Chen X, Lopresti BJ, et al. The high affinity peripheral benzodiazepine receptor ligand DAA1106 binds specifically to microglia in a rat model of traumatic brain injury: implications for PET imaging. *Exp Neurol* 2007;**207**:118−27.
111. Gulyás B, Makkai B, Kása P, Gulya K, Bakota L, Várszegi S, et al. A comparative autoradiography study in post mortem whole hemisphere human brain slices taken from Alzheimer patients and age-matched controls using two radiolabelled DAA1106 analogues with high affinity to the peripheral benzodiazepine receptor (PBR) system. *Neurochem Int* 2009;**54**:28−36.
112. Yasuno F, Ota M, Kosaka J, Ito H, Higuchi M, Doronbekov TK, et al. Increased binding of peripheral benzodiazepine receptor in Alzheimer's disease measured by positron emission tomography with [^{11}C]DAA1106. *Biol Psychiatr* 2008;**64**:835−41.
113. Yasuno F, Kosaka J, Ota M, Higuchi M, Ito H, Fujimura Y, et al. Increased binding of peripheral benzodiazepine receptor in mild cognitive impairment-dementia converters measured by positron emission tomography with [^{11}C]DAA1106. *Psychiatr Res* 2012;**203**:67−74.
114. Kumata K, Zhang Y, Fujinaga M, Ohkubo T, Mori W, Yamasaki T, et al. [^{18}F]DAA1106: automated radiosynthesis using spirocyclic iodonium ylide and preclinical evaluation for positron emission tomography imaging of translocator protein (18kDa). *Bioorg Med Chem* 2018;**26**:4817−22.
115. Zhang MR, Maeda J, Furutsuka K, Yoshida Y, Ogawa M, Suhara T, et al. [^{18}F]FMDAA1106 and [^{18}F]FEDAA1106: two positron-emitter labeled ligands for peripheral benzodiazepine receptor (PBR). *Bioorg Med Chem Lett* 2003;**13**:201−4.

116. Zhang MR, Maeda J, Ogawa M, Noguchi J, Ito T, Yoshida Y, et al. Development of a new radioligand, *N*-(5-fluoro-2-phenoxyphenyl)-*N*-(2-[^{18}F]fluoroethyl-5-methoxybenzyl)acetamide, for PET imaging of peripheral benzodiazepine receptor in primate brain. *J Med Chem* 2004;**47**:2228−35.
117. Maeda J, Ji B, Irie T, Tomiyama T, Maruyama M, Okauchi T, et al. Longitudinal, quantitative assessment of amyloid, neuroinflammation, and anti-amyloid treatment in a living mouse model of Alzheimer's disease enabled by positron emission tomography. *J Neurosci* 2007;**27**:10957−68.
118. Varrone A, Mattsson P, Forsberg A, Takano A, Nag S, Gulyás B, et al. *In vivo* imaging of the 18-kDa translocator protein (TSPO) with [^{18}F]FEDAA1106 and PET does not show increased binding in Alzheimer's disease patients. *Eur J Nucl Med Mol Imag* 2013;**40**:921−31.
119. Takano A, Piehl F, Hillert J, Varrone A, Nag S, Gulyás B, et al. *In vivo* TSPO imaging in patients with multiple sclerosis: a brain PET study with [^{18}F]FEDAA1106. *EJNMMI Res* 2013;**3**:30.
120. Briard E, Zoghbi SS, Imaizumi M, Gourley JP, Shetty HU, Hong J, et al. Synthesis and evaluation in monkey of two sensitive ^{11}C-labeled aryloxyanilide ligands for imaging brain peripheral benzodiazepine receptors *in vivo*. *J Med Chem* 2008;**51**:17−30.
121. Imaizumi M, Briard E, Zoghbi SS, Gourley JP, Hong J, Fujimura Y, et al. Brain and whole-body imaging in nonhuman primates of [^{11}C]PBR28, a promising PET radioligand for peripheral benzodiazepine receptors. *Neuroimage* 2008;**39**:1289−98.
122. Kreisl WC, Fujita M, Fujimura Y, Kimura N, Jenko KJ, Kannan P, et al. Comparison of [^{11}C]-(R)-PK 11195 and [^{11}C]PBR28, two radioligands for translocator protein (18 kDa) in human and monkey: implications for positron emission tomographic imaging of this inflammation biomarker. *Neuroimage* 2010;**49**:2924−32.
123. Brown AK, Fujita M, Fujimura Y, Liow JS, Stabin M, Ryu YH, et al. Radiation dosimetry and biodistribution in monkey and man of ^{11}C-PBR28: a PET radioligand to image inflammation. *J Nucl Med* 2007;**48**:2072−9.
124. Oh U, Fujita M, Ikonomidou VN, Evangelou IE, Matsuura E, Harberts E, et al. Translocator protein PET imaging for glial activation in multiple sclerosis. *J Neuroimmune Pharmacol* 2011;**6**:354−61.
125. Hirvonen J, Kreisl WC, Fujita M, Dustin I, Khan O, Appel S, et al. Increased *in vivo* expression of an inflammatory marker in temporal lobe epilepsy. *J Nucl Med* 2012;**53**:234−40.
126. Lyoo CH, Ikawa M, Liow JS, Zoghbi SS, Morse CL, Pike VW, et al. Cerebellum can serve as a pseudo-reference region in Alzheimer disease to detect neuroinflammation measured with PET radioligand binding to translocator protein. *J Nucl Med* 2015;**56**:701−6.
127. Kreisl WC, Lyoo CH, Liow JS, Wei M, Snow J, Page E, et al. ^{11}C-PBR28 binding to translocator protein increases with progression of Alzheimer's disease. *Neurobiol Aging* 2016;**44**:53−61.
128. Kreisl WC, Lyoo CH, Liow JS, Snow J, Page E, Jenko KJ, et al. Distinct patterns of increased translocator protein in posterior cortical atrophy and amnestic Alzheimer's disease. *Neurobiol Aging* 2017;**51**:132−40.
129. Lois C, González I, Izquierdo-García D, Zürcher NR, Wilkens P, Loggia ML, et al. Neuroinflammation in Huntington's disease: new insights with ^{11}C-PBR28 PET/MRI. *ACS Chem Neurosci* 2018;**9**:2563−71.
130. Alshikho MJ, Zürcher NR, Loggia ML, Cernasov P, Reynolds B, Pijanowski O, et al. Integrated magnetic resonance imaging and [^{11}C]-PBR28 positron emission tomographic imaging in amyotrophic lateral sclerosis. *Ann Neurol* 2018;**83**:1186−97.
131. Zürcher NR, Loggia ML, Lawson R, Chonde DB, Izquierdo-Garcia D, Yasek JE, et al. Increased *in vivo* glial activation in patients with amyotrophic lateral sclerosis: assessed with [^{11}C]-PBR28. *Neuroimage Clin* 2015;**7**:409−14.
132. Ratai EM, Alshikho MJ, Zürcher NR, Loggia ML, Cebulla CL, Cernasov P, et al. Integrated imaging of [^{11}C]-PBR28 PET, MR diffusion and magnetic resonance spectroscopy ^{1}H-MRS in amyotrophic lateral sclerosis. *Neuroimage Clin* 2018;**20**:357−64.
133. Dickstein LP, Zoghbi SS, Fujimura Y, Imaizumi M, Zhang Y, Pike VW, et al. Comparison of ^{18}F- and ^{11}C-labeled aryloxyanilide analogs to measure translocator protein in human brain using positron emission tomography. *Eur J Nucl Med Mol Imag* 2011;**38**:352−7.
134. Imaizumi M, Briard E, Zoghbi SS, Gourley JP, Hong J, Musachio JL, et al. Kinetic evaluation in nonhuman primates of two new PET ligands for peripheral benzodiazepine receptors in brain. *Synapse* 2007;**61**:595−605.
135. Lartey FM, Ahn GO, Shen B, Cord KT, Smith T, Chua JY, et al. PET imaging of stroke-induced neuroinflammation in mice using [^{18}F]PBR06. *Mol Imag Biol* 2014;**16**:109−17.
136. James ML, Belichenko NP, Nguyen TV, Andrews LE, Ding Z, Liu H, et al. PET imaging of translocator protein (18 kDa) in a mouse model of Alzheimer's disease using *N*-(2,5-dimethoxybenzyl)-2-^{18}F-fluoro-*N*-(2-phenoxyphenyl)acetamide. *J Nucl Med* 2015;**56**:311−6.
137. Simmons DA, James ML, Belichenko NP, Semaan S, Condon C, Kuan J, et al. TSPO-PET imaging using [^{18}F]PBR06 is a potential translatable biomarker for treatment response in Huntington's disease: preclinical evidence with the p75NTR ligand LM11A-31. *Hum Mol Genet* 2018;**27**:2893−912.
138. Fujimura Y, Zoghbi SS, Simèon FG, Taku A, Pike VW, Innis RB, et al. Quantification of translocator protein (18 kDa) in the human brain with PET and a novel radioligand, ^{18}F-PBR06. *J Nucl Med* 2009;**50**:1047−53.
139. Fujimura Y, Kimura Y, Siméon FG, Dickstein LP, Pike VW, Innis RB, et al. Biodistribution and radiation dosimetry in humans of a new PET ligand, ^{18}F-PBR06, to image translocator protein (18 kDa). *J Nucl Med* 2010;**51**:145−9.
140. Rusjan PM, Wilson AA, Bloomfield PM, Vitcu I, Meyer JH, Houle S, et al. Quantitation of translocator protein binding in human brain with the novel radioligand [^{18}F]FEPPA and positron emission tomography. *J Cerebr Blood Flow Metabol* 2011;**31**:1807−16.
141. Suridjan I, Pollock BG, Verhoeff NP, Voineskos AN, Chow T, Rusjan PM, et al. *In-vivo* imaging of grey and white matter neuroinflammation in Alzheimer's disease: a positron emission tomography study with a novel radioligand, [^{18}F]-FEPPA. *Mol Psychiatr* 2015;**20**:1579−87.
142. Setiawan E, Attwells S, Wilson AA, Mizrahi R, Rusjan PM, Miler L, et al. Association of translocator protein total distribution volume with duration of untreated major depressive disorder: a cross-sectional study. *Lancet Psychiatry* 2018;**5**:339−47.
143. Holmes SE, Hinz R, Conen S, Gregory CJ, Matthews JC, Anton-Rodriguez JM, et al. Elevated translocator protein in anterior cingulate in major depression and a role for inflammation in suicidal thinking: a positron emission tomography study. *Biol Psychiatr* 2018;**83**:61−9.
144. Richards EM, Zanotti-Fregonara P, Fujita M, Newman L, Farmer C, Ballard ED, et al. PET radioligand binding to translocator protein (TSPO) is increased in unmedicated depressed subjects. *EJNMMI Res* 2018;**8**:57.
145. Li H, Sagar AP, Kéri S. Microglial markers in the frontal cortex are related to cognitive dysfunctions in major depressive disorder. *J Affect Disord* 2018;**241**:305−10.
146. Li H, Sagar AP, Kéri S. Translocator protein (18 kDa TSPO) binding, a marker of microglia, is reduced in major depression during cognitive-behavioral therapy. *Prog Neuro-Psychopharmacol Biol Psychiatry* 2018;**83**:1−7.
147. Dollé F, Hinnen F, Damont A, Kuhnast B, Fookes C, Pham T, et al. Radiosynthesis of [^{18}F]PBR111, a selective radioligand for imaging the translocator protein (18 kDa) with PET. *J Label Compd Radiopharm* 2008;**51**:435−9.
148. Fookes CJ, Pham TQ, Mattner F, Greguric I, Loc'h C, Liu X, et al. Synthesis and biological evaluation of substituted [^{18}F]imidazo[1,2-*a*]pyridines and [^{18}F]pyrazolo[1,5-*a*]pyrimidines for the study of the

peripheral benzodiazepine receptor using positron emission tomography. *J Med Chem* 2008;**51**:3700−12.
149. Van Camp N, Boisgard R, Kuhnast B, Thézé B, Viel T, Grégoire MC, et al. *In vivo* imaging of neuroinflammation: a comparative study between [^{18}F]PBR111, [^{11}C]CLINME and [^{11}C]PK11195 in an acute rodent model. *Eur J Nucl Med Mol Imag* 2010;**37**:962−72.
150. Guo Q, Colasanti A, Owen DR, Onega M, Kamalakaran A, Bennacef I, et al. Quantification of the specific translocator protein signal of ^{18}F-PBR111 in healthy humans: a genetic polymorphism effect on *in vivo* binding. *J Nucl Med* 2013;**54**:1915−23.
151. Hatano K, Sekimata K, Yamada T, Abe J, Ito K, Ogawa M, et al. Radiosynthesis and *in vivo* evaluation of two imidazopyridineacetamides, [^{11}C]CB184 and [^{11}C]CB190, as a PET tracer for 18 kDa translocator protein: direct comparison with [^{11}C](R)-PK11195. *Ann Nucl Med* 2015;**29**:325−35.
152. Vállez Garcia D, de Vries EF, Toyohara J, Ishiwata K, Hatano K, Dierckx RA, et al. Evaluation of [^{11}C]CB184 for imaging and quantification of TSPO overexpression in a rat model of herpes encephalitis. *Eur J Nucl Med Mol Imag* 2015;**42**:1106−18.
153. Toyohara J, Sakata M, Hatano K, Yanai S, Endo S, Ishibashi K, et al. Preclinical and first-in-man studies of [^{11}C]CB184 for imaging the 18-kDa translocator protein by positron emission tomography. *Ann Nucl Med* 2016;**30**:534−43.
154. Sakata M, Ishibashi K, Imai M, Wagatsuma K, Ishii K, Hatano K, et al. Assessment of safety, efficacy, and dosimetry of a novel 18-kDa translocator protein ligand, [^{11}C]CB184, in healthy human volunteers. *EJNMMI Res* 2017;**7**:26.
155. Yanamoto K, Zhang MR. *N*-Benzyl-*N*-ethyl-2-(7-[^{11}C]-methyl-8-oxo-2-phenyl-7,8-dihydro-9*H*-purin-9-yl)acetamide. In: *Molecular imaging and contrast agent database (MICAD) [internet]*. Bethesda (MD): National Center for Biotechnology Information (US); 2004–2013. Available from: https://pubmed.ncbi.nlm.nih.gov/20641683.
156. Kita A, Kohayakawa H, Kinoshita T, Ochi Y, Nakamichi K, Kurumiya S, et al. Antianxiety and antidepressant-like effects of AC-5216, a novel mitochondrial benzodiazepine receptor ligand. *Br J Pharmacol* 2004;**142**:1059−72.
157. Yanamoto K, Zhang MR, Kumata K, Hatori A, Okada M, Suzuki K. *In vitro* and *ex vivo* autoradiography studies on peripheral-type benzodiazepine receptor binding using [^{11}C]AC-5216 in normal and kainic acid-lesioned rats. *Neurosci Lett* 2007;**428**:59−63.
158. Yanamoto K, Yamasaki T, Kumata K, Yui J, Odawara C, Kawamura K, et al. Evaluation of *N*-benzyl-*N*-[^{11}C]methyl-2-(7-methyl-8-oxo-2-phenyl-7,8-dihydro-9*H*-purin-9-yl)acetamide([^{11}C]DAC) as a novel translocator protein (18 kDa) radioligand in kainic acid-lesioned rat. *Synapse* 2009;**63**:961−71.
159. Trapani A, Palazzo C, de Candia M, Lasorsa FM, Trapani G. Targeting of the translocator protein 18 kDa (TSPO): a valuable approach for nuclear and optical imaging of activated microglia. *Bioconjugate Chem* 2013;**24**:1415−28.
160. James ML, Fulton RR, Henderson DJ, Eberl S, Meikle SR, Thomson S, et al. Synthesis and *in vivo* evaluation of a novel peripheral benzodiazepine receptor PET radioligand. *Bioorg Med Chem* 2005;**13**:6188−94.
161. Boutin H, Chauveau F, Thominiaux C, Grégoire MC, James ML, Trebossen R, et al. ^{11}C-DPA-713: a novel peripheral benzodiazepine receptor PET ligand for *in vivo* imaging of neuroinflammation. *J Nucl Med* 2007;**48**:573−81.
162. Chauveau F, Van Camp N, Dollé F, Kuhnast B, Hinnen F, Damont A, et al. Comparative evaluation of the translocator protein radioligands ^{11}C-DPA-713, ^{18}F-DPA-714, and ^{11}C-PK11195 in a rat model of acute neuroinflammation. *J Nucl Med* 2009;**50**:468−76.
163. Chaney AM, Johnson EM, Cropper HC, James ML. PET imaging of neuroinflammation using [^{11}C]DPA-713 in a mouse model of ischemic stroke. *JoVE* 2018:e57243.
164. Chaney A, Cropper HC, Johnson EM, Lechtenberg KJ, Peterson TC, Stevens MY, et al. ^{11}C-DPA-713 *versus* ^{18}F-GE-180: a preclinical comparison of translocator protein 18 kDa PET tracers to visualize acute and chronic neuroinflammation in a mouse model of ischemic stroke. *J Nucl Med* 2019;**60**:122−8.
165. Endres CJ, Pomper MG, James M, Uzuner O, Hammoud DA, Watkins CC, et al. Initial evaluation of ^{11}C-DPA-713, a novel TSPO PET ligand, in humans. *J Nucl Med* 2009;**50**:1276−82.
166. Endres CJ, Coughlin JM, Gage KL, Watkins CC, Kassiou M, Pomper MG. Radiation dosimetry and biodistribution of the TSPO ligand ^{11}C-DPA-713 in humans. *J Nucl Med* 2012;**53**:330−5.
167. James ML, Fulton RR, Vercoullie J, Henderson DJ, Garreau L, Chalon S, et al. DPA-714, a new translocator protein-specific ligand: synthesis, radiofluorination, and pharmacologic characterization. *J Nucl Med* 2008;**49**:814−22.
168. Ory D, Postnov A, Koole M, Celen S, de Laat B, Verbruggen A, et al. Quantification of TSPO overexpression in a rat model of local neuroinflammation induced by intracerebral injection of LPS by the use of [^{18}F]DPA-714 PET. *Eur J Nucl Med Mol Imag* 2016;**43**:163−72.
169. Doorduin J, Klein HC, Dierckx RA, James M, Kassiou M, de Vries EF. [^{11}C]-DPA-713 and [^{18}F]-DPA-714 as new PET tracers for TSPO: a comparison with [^{11}C]-(*R*)-PK11195 in a rat model of herpes encephalitis. *Mol Imag Biol* 2009;**11**:386−98.
170. Thomas C, Vercouillie J, Doméné A, Tauber C, Kassiou M, Guilloteau D, et al. Detection of neuroinflammation in a rat model of subarachnoid hemorrhage using [^{18}F]DPA-714 PET imaging. *Mol Imag* 2016;**15**:1536012116639189.
171. Gargiulo S, Anzilotti S, Coda AR, Gramanzini M, Greco A, Panico M, et al. Imaging of brain TSPO expression in a mouse model of amyotrophic lateral sclerosis with ^{18}F-DPA-714 and micro-PET/CT. *Eur J Nucl Med Mol Imag* 2016;**43**:1348−59.
172. Miyajima N, Ito M, Rokugawa T, Iimori H, Momosaki S, Omachi S, et al. Detection of neuroinflammation before selective neuronal loss appearance after mild focal ischemia using [^{18}F]DPA-714 imaging. *EJNMMI Res* 2018;**8**:43.
173. Tan C, Zhao S, Higashikawa K, Wang Z, Kawabori M, Abumiya T, et al. [^{18}F]DPA-714 PET imaging shows immunomodulatory effect of intravenous administration of bone marrow stromal cells after transient focal ischemia. *EJNMMI Res* 2018;**8**:35.
174. Nguyen DL, Wimberley C, Truillet C, Jego B, Caillé F, Pottier G, et al. Longitudinal positron emission tomography imaging of glial cell activation in a mouse model of mesial temporal lobe epilepsy: toward identification of optimal treatment windows. *Epilepsia* 2018;**59**:1234−44.
175. Arlicot N, Vercouillie J, Ribeiro MJ, Tauber C, Venel Y, Baulieu JL, et al. Initial evaluation in healthy humans of [^{18}F]DPA-714, a potential PET biomarker for neuroinflammation. *Nucl Med Biol* 2012;**39**:570−8.
176. Golla SS, Boellaard R, Oikonen V, Hoffmann A, van Berckel BN, Windhorst AD, et al. Parametric binding images of the TSPO ligand ^{18}F-DPA-714. *J Nucl Med* 2016;**57**:1543−7.
177. Hamelin L, Lagarde J, Dorothée G, Leroy C, Labit M, Comley RA, et al. Early and protective microglial activation in Alzheimer's disease: a prospective study using ^{18}F-DPA-714 PET imaging. *Brain* 2016;**139**:1252−64.
178. Hagens MHJ, Golla SV, Wijburg MT, Yaqub M, Heijtel D, Steenwijk MD, et al. *In vivo* assessment of neuroinflammation in progressive multiple sclerosis: a proof of concept study with [^{18}F]DPA714 PET. *J Neuroinflammation* 2018;**15**:314.
179. Wang L, Cheng R, Fujinaga M, Yang J, Zhang Y, Hatori A, et al. A facile radiolabeling of [^{18}F]FDPA *via* spirocyclic iodonium ylides: preliminary PET imaging studies in preclinical models of neuroinflammation. *J Med Chem* 2017;**60**:5222−7.
180. Keller T, López-Picón FR, Krzyczmonik A, Forsback S, Kirjavainen AK, Takkinen JS, et al. [^{18}F] F-DPA for the detection of activated microglia in a mouse model of Alzheimer's disease. *Nucl Med Biol* 2018;**67**:1−9.
181. Tang D, Li J, Nickels ML, Huang G, Cohen AS, Manning HC. Preclinical evaluation of a novel TSPO PET ligand 2-(7-butyl-2-(4-(2-[^{18}F]fluoroethoxy) phenyl)-5-methylpyrazolo [1,5-*a*] pyrimidin-3-

yl) -*N,N*-diethylacetamide (^{18}F-VUIIS1018A) to image glioma. *Mol Imag Biol* 2019;**21**:113−21.
182. Gulyás B, Halldin C, Karlsson P, Chou YH, Swahn CG, Bonock P, et al. Brain uptake and plasma metabolism of [^{11}C]vinpocetine: a preliminary PET study in a cynomolgus monkey. *J Neuroimaging* 1999;**9**:217−22.
183. Gulyás B, Halldin C, Sandell J, Karlsson P, Sóvágó J, Kárpáti E, et al. PET studies on the brain uptake and regional distribution of [^{11}C] vinpocetine in human subjects. *Acta Neurol Scand* 2002;**106**: 325−32.
184. Vas A, Shchukin Y, Karrenbauer VD, Cselényi Z, Kostulas K, Hillert J, et al. Functional neuroimaging in multiple sclerosis with radiolabelled glia markers: preliminary comparative PET studies with [^{11}C]vinpocetine and [^{11}C]PK11195 in patients. *J Neurol Sci* 2008;**264**:9−17.
185. Gulyás B, Vas A, Tóth M, Takano A, Varrone A, Cselényi Z, et al. Age and disease related changes in the translocator protein (TSPO) system in the human brain: positron emission tomography measurements with [^{11}C]vinpocetine. *Neuroimage* 2011;**56**:1111−21.
186. Fujinaga M, Kumata K, Zhang Y, Hatori A, Yamasaki T, Mori W, et al. Synthesis of two novel [^{18}F]fluorobenzene-containing radiotracers *via* spirocyclic iodonium ylides and positron emission tomography imaging of translocator protein (18 kDa) in ischemic brain. *Org Biomol Chem* 2018;**16**:8325−35.
187. Yui J, Maeda J, Kumata K, Kawamura K, Yanamoto K, Hatori A, et al. ^{18}F-FEAC and ^{18}F-FEDAC: PET of the monkey brain and imaging of translocator protein (18 kDa) in the infarcted rat brain. *J Nucl Med* 2010;**51**:1301−9.
188. Yanamoto K, Kumata K, Yamasaki T, Odawara C, Kawamura K, Yui J, et al. [^{18}F]FEAC and [^{18}F]FEDAC: two novel positron emission tomography ligands for peripheral-type benzodiazepine receptor in the brain. *Bioorg Med Chem Lett* 2009;**19**:1707−10.
189. Tiwari AK, Yui J, Fujinaga M, Kumata K, Shimoda Y, Yamasaki T, et al. Characterization of a novel acetamidobenzoxazolone-based PET ligand for translocator protein (18 kDa) imaging of neuroinflammation in the brain. *J Neurochem* 2014;**129**:712−20.
190. Varrone A, Oikonen V, Forsberg A, Joutsa J, Takano A, Solin O, et al. Positron emission tomography imaging of the 18-kDa translocator protein (TSPO) with [^{18}F]FEMPA in Alzheimer's disease patients and control subjects. *Eur J Nucl Med Mol Imag* 2015;**42**:438−46.
191. Owen DR, Gunn RN, Rabiner EA, Bennacef I, Fujita M, Kreisl WC, et al. Mixed-affinity binding in humans with 18-kDa translocator protein ligands. *J Nucl Med* 2011;**52**:24−32.
192. Zanotti-Fregonara P, Zhang Y, Jenko KJ, Gladding RL, Zoghbi SS, Fujita M, et al. Synthesis and evaluation of translocator 18 kDa protein (TSPO) positron emission tomography (PET) radioligands with low binding sensitivity to human single nucleotide polymorphism *rs6971*. *ACS Chem Neurosci* 2014;**5**:963−71.
193. Owen DR, Yeo AJ, Gunn RN, Song K, Wadsworth G, Lewis A, et al. An 18-kDa translocator protein (TSPO) polymorphism explains differences in binding affinity of the PET radioligand PBR28. *J Cerebr Blood Flow Metabol* 2012;**32**:1−5.
194. Tiwari AK, Fujinaga M, Yui J, Yamasaki T, Xie L, Kumata K, et al. Synthesis and evaluation of new ^{18}F-labelled acetamidobenzoxazolone-based radioligands for imaging of the translocator protein (18 kDa, TSPO) in the brain. *Org Biomol Chem* 2014;**12**:9621−30.
195. Tiwari AK, Ji B, Yui J, Fujinaga M, Yamasaki T, Xie L, et al. [^{18}F] FEBMP: positron emission tomography imaging of TSPO in a model of neuroinflammation in rats, and *in vitro* autoradiograms of the human brain. *Theranostics* 2015;**5**:961−9.
196. Fan Z, Calsolaro V, Atkinson RA, Femminella GD, Waldman A, Buckley C, et al. Flutriciclamide (^{18}F-GE180) PET: first-in-human PET study of novel third-generation *in vivo* marker of human translocator protein. *J Nucl Med* 2016;**57**:1753−9.
197. Wadsworth H, Jones PA, Chau WF, Durrant C, Fouladi N, Passmore J, et al. [^{18}F]GE-180: a novel fluorine-18 labelled PET tracer for imaging translocator protein 18 kDa (TSPO). *Bioorg Med Chem Lett* 2012;**22**:1308−13.
198. Dickens AM, Vainio S, Marjamäki P, Johansson J, Lehtiniemi P, Rokka J, et al. Detection of microglial activation in an acute model of neuroinflammation using PET and radiotracers ^{11}C-(*R*)-PK11195 and ^{18}F-GE-180. *J Nucl Med* 2014;**55**:466−72.
199. Boutin H, Murray K, Pradillo J, Maroy R, Smigova A, Gerhard A, et al. ^{18}F-GE-180: a novel TSPO radiotracer compared to ^{11}C-R-PK11195 in a preclinical model of stroke. *Eur J Nucl Med Mol Imag* 2015;**42**:503−11.
200. Liu B, Le KX, Park MA, Wang S, Belanger AP, Dubey S, et al. *In vivo* detection of age- and disease-related increases in neuroinflammation by ^{18}F-GE180 TSPO microPET imaging in wild-type and Alzheimer's transgenic mice. *J Neurosci* 2015;**35**:15716−30.
201. López-Picón FR, Snellman A, Eskola O, Helin S, Solin O, Haaparanta-Solin M, et al. Neuroinflammation appears early on PET imaging and then plateaus in a mouse model of Alzheimer disease. *J Nucl Med* 2018;**59**:509−15.
202. Russmann V, Brendel M, Mille E, Helm-Vicidomini A, Beck R, Günther L, et al. Identification of brain regions predicting epileptogenesis by serial [^{18}F]GE-180 positron emission tomography imaging of neuroinflammation in a rat model of temporal lobe epilepsy. *Neuroimage Clin* 2017;**15**:35−44.
203. Feeney C, Scott G, Raffel J, Roberts S, Coello C, Jolly A, et al. Kinetic analysis of the translocator protein positron emission tomography ligand [^{18}F]GE-180 in the human brain. *Eur J Nucl Med Mol Imag* 2016;**43**:2201−10.
204. Vomacka L, Albert NL, Lindner S, Unterrainer M, Mahler C, Brendel M, et al. TSPO imaging using the novel PET ligand [^{18}F] GE-180: quantification approaches in patients with multiple sclerosis. *EJNMMI Res* 2017;**7**:89.
205. Unterrainer M, Mahler C, Vomacka L, Lindner S, Havla J, Brendel M, et al. TSPO PET with [^{18}F]GE-180 sensitively detects focal neuroinflammation in patients with relapsing-remitting multiple sclerosis. *Eur J Nucl Med Mol Imag* 2018;**45**:1423−31.
206. Zanotti-Fregonara P, Pascual B, Rizzo G, Yu M, Pal N, Beers D, et al. Head-to-head comparison of ^{11}C-PBR28 and ^{18}F-GE180 for quantification of the translocator protein in the human brain. *J Nucl Med* 2018;**59**:1260−6.
207. Ikawa M, Lohith TG, Shrestha S, Telu S, Zoghbi SS, Castellano S, et al. ^{11}C-ER176, a radioligand for 18-kDa translocator protein, has adequate sensitivity to robustly image all three affinity genotypes in human brain. *J Nucl Med* 2017;**58**:320−5.
208. Fujita M, Kobayashi M, Ikawa M, Gunn RN, Rabiner EA, Owen DR, et al. Comparison of four ^{11}C-labeled PET ligands to quantify translocator protein 18 kDa (TSPO) in human brain: (*R*)-PK11195, PBR28, DPA-713, and ER176-based on recent publications that measured specific-to-non-displaceable ratios. *EJNMMI Res* 2017;**7**: 84.
209. Qiao L, Fisher E, McMurray L, Milicevic Sephton S, Hird M, Kuzhuppilly-Ramakrishnan N, et al. Radiosynthesis of (*R,S*)-[^{18}F] GE387: a potential PET radiotracer for imaging translocator protein 18 kDa (TSPO) with low binding sensitivity to the human gene polymorphism *rs6971*. *ChemMedChem* 2019;**14**:982−93.
210. Lu S, Haskali MB, Ruley KM, Dreyfus NJ, DuBois SL, Paul S, et al. PET ligands [^{18}F]LSN3316612 and [^{11}C]LSN3316612 quantify *O*-linked-β-*N*-acetyl-glucosamine hydrolase in the brain. *Sci Transl Med* 2020;**12**:eaau2939.
211. Jaremko M, Jaremko Ł, Giller K, Becker S, Zweckstetter M. Structural integrity of the A147T polymorph of mammalian TSPO. *Chembiochem* 2015;**16**:1483−9.
212. Jaremko M, Jaremko Ł, Jaipuria G, Becker S, Zweckstetter M. Structure of the mammalian TSPO/PBR protein. *Biochem Soc Trans* 2015;**43**:566−71.
213. Betlazar C, Harrison-Brown M, Middleton RJ, Banati R, Liu GJ. Cellular sources and regional variations in the expression of the neuroinflammatory marker translocator protein (TSPO) in the normal brain. *Int J Mol Sci* 2018;**19**:18.
214. Narayanaswami V, Dahl K, Bernard-Gauthier V, Josephson L, Cumming P, Vasdev N. Emerging PET radiotracers and targets for

imaging of neuroinflammation in neurodegenerative diseases: outlook beyond TSPO. *Mol Imag* 2018;**17**:1536012118792317.
215. Horti AG, Naik R, Foss CA, Minn I, Misheneva V, Du Y, et al. PET imaging of microglia by targeting macrophage colony-stimulating factor 1 receptor (CSF1R). *Proc Natl Acad Sci U S A* 2019;**116**:1686−91.
216. Cumming P, Burgher B, Patkar O, Breakspear M, Vasdev N, Thomas P, et al. Sifting through the surfeit of neuroinflammation tracers. *J Cerebr Blood Flow Metabol* 2018;**38**:204−24.
217. Berdyyeva T, Xia C, Taylor N, He Y, Chen G, Huang C, et al. PET imaging of the $P2X_7$ ion channel with a novel tracer [^{18}F]JNJ-64413739 in a rat model of neuroinflammation. *Mol Imag Biol* 2019;**21**:871−8.
218. Van Weehaeghe D, Van Schoor E, De Vocht J, Koole M, Attili B, Celen S, et al. TSPO *versus* $P2X_7$ as target for neuroinflammation: an *in vitro* and *in vivo* study. *J Nucl Med* 2019;**61**:604−7.
219. Van Weehaeghe D, Koole M, Schmidt ME, Deman S, Jacobs AH, Souche E, et al. [^{11}C]JNJ54173717, a novel $P2X_7$ receptor radioligand as marker for neuroinflammation: human biodistribution, dosimetry, brain kinetic modelling and quantification of brain $P2X_7$ receptors in patients with Parkinson's disease and healthy volunteers. *Eur J Nucl Med Mol Imag* 2019;**46**:2051−64.
220. Vasdev N, Sadovski O, Garcia A, Dollé F, Meyer JH, Houle S, et al. Radiosynthesis of [^{11}C]SL25.1188 *via* [^{11}C]CO2 fixation for imaging monoamine oxidase B. *J Label Compd Radiopharm* 2011;**54**:678−80.
221. Moriguchi S, Wilson AA, Miler L, Rusjan PM, Vasdev N, Kish SJ, et al. Monoamine oxidase B total distribution volume in the prefrontal cortex of major depressive disorder: an [^{11}C] SL25.1188 positron emission tomography study. *JAMA Psychiatry* 2019;**76**:634−41.